RI 9231

REPORT OF INVESTIGATIONS/1989

In Situ Measurements and Preliminary Design Analysis for Deep Mine Shafts in Highly Stressed Rock

By M. P. Board and M. J. Beus

BUREAU OF MINES

UNITED STATES DEPARTMENT OF THE INTERIOR

Report of Investigations 9231

In Situ Measurements and Preliminary Design Analysis for Deep Mine Shafts in Highly Stressed Rock

By M. P. Board and M. J. Beus

UNITED STATES DEPARTMENT OF THE INTERIOR
Manuel J. Lujan, Jr., Secretary

BUREAU OF MINES
T S Ary, Director

Library of Congress Cataloging in Publication Data:

Board, M. P. (Mark P.)
In situ measurements and preliminary design analysis for deep mine shafts in highly stressed rock.

(Report of investigations / United States Department of the Interior, Bureau of Mines; 9231)

Bibliography: p. 20.

Supt. of Docs. no.: I 28.23:9231.

1. Shaft sinking. 2. Rock deformation—Idaho—Coeur d'Alene Region. 3. Ground control—Idaho—Coeur d'Alene Region. I. Beus, Michael J. II. Title. III. Report of investigations (United States. Bureau of Mines); 9231.

TN23.U43 [TN283] 622 s [62'.25] 88-600304

CONTENTS

ILLUSTRATIONS

ILLUSTRATIONS–Continued

TABLES

UNIT OF MEASURE ABBREVIATIONS USED IN THIS REPORT

cm	centimeter	μin/in	microinch per inch
°C	degree Celsius	oz	ounce
deg	degree	pct	percent
ft	foot	lb/ft^3	pound per cubic foot
ft/d	foot per day	psi	pound per square inch
GPa	gigapascal	tr oz	troy ounce
h	hour	yd^3	cubic yard
in	inch	yr	year
$\mu\epsilon$	microstrain ($\epsilon \times 10^6$)		

IN SITU MEASUREMENTS AND PRELIMINARY DESIGN ANALYSIS FOR DEEP MINE SHAFTS IN HIGHLY STRESSED ROCK

By M. P. Board[1] and M. J. Beus[2]

ABSTRACT

The U.S. Bureau of Mines, under a cooperative agreement with Hecla Mining Co., conducted a rock mechanics study at four widely spaced horizons in a deep mine shaft in northern Idaho. The objective of the project was to measure and analyze rock deformation and lining behavior during construction of a deep shaft in a high in situ stress field within an isotropic rock mass. Rock mass displacements were monitored with multiple-position borehole extensometers. Liner stress and strain were measured with concrete pressure cells and embedment strain gauges.

This report discusses the general trends and magnitudes of data from the four test sites, and relates the data to a proposed anisotropic constitutive model for the rock mass. A design procedure is then outlined for specifications of liner thickness and support installation sequences for future shaft sinking.

[1]Ph.D. candidate, University of Minnesota, Minneapolis, MN.
[2]Mining engineer, Spokane Research Center, U.S. Bureau of Mines, Spokane, WA.

INTRODUCTION

The shaft is truly the "lifeline" of an underground mine. Damage to the shaft lining and guides as a result of ground movement can necessitate extensive and continual repair, which in turn causes serious loss of production. In the Coeur d'Alene Mining District of northern Idaho (fig. 1), the problems caused by high horizontal in situ stress, and the resulting ground control problems, have been documented (*4, 11*).[3] Rectangular shafts supported by wooden sets and oriented with the long axis normal to the bedding are the rule. In many cases, these shafts have been sunk close to active stoping areas. The bedded and heavily jointed nature of the quartzites of the district, combined with stress concentrations from surrounding workings, have resulted in rather extensive repair problems.

[3]Italic numbers in parentheses refer to items in the list of references preceding the appendixes at the end of this report.

To service the deep extensions of the Lucky Friday ore body, in 1979 Hecla Mining Co. made the decision to sink a circular, concrete-lined shaft from the surface. This shaft was unique to the district in that it was the first circular concrete-lined shaft. Excavation of the shaft was initiated in 1980 by the J. S. Redpath Corp. and completed in 1983 to a total depth of 6,200 ft (*14*).

Four test sites at shaft depths of 2,414, 4,063, 5,191, and 5,955 ft were instrumented by the Bureau of Mines. Reference dates from which to calculate the collection of data were established as follows: test sites 1 and 2–December 31, 1980; test site 3–December 31, 1981; test site 4–December 31, 1982. This report analyzes the data from these four sites and describes their relevance to shaft design. Based on these data, a general procedure for concrete liner design in the Coeur d'Alene Mining District is given.

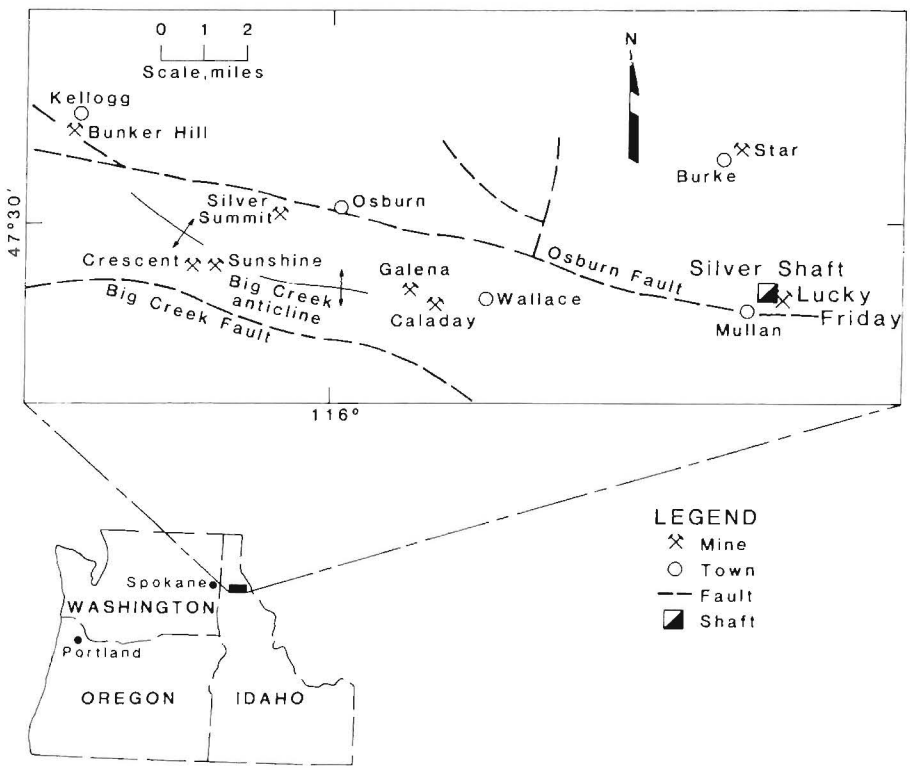

Figure 1.–Coeur d'Alene Mining District and location of Lucky Friday Mine and Silver Shaft.

ACKNOWLEDGMENTS

The authors express their gratitude to officials and personnel of Hecla Mining Co., particularly P. Boyko, project manager; C. Flood and T. Stephenson, mining technicians; and J. S. Redpath Corp., the shaft-sinking contractor, for assistance with installation of the instruments.

Further thanks go to mining engineers R. Muhs and J. K. Whyatt and supervisory electronics technician J. R. McVey of the Spokane Research Center (SRC); E. Hardin, geophysicist, of Science Applications, Inc., for computer hardware and software development, data processing, and assistance with instrument preparation and installation; and N. Barton and K. Bahktar, both formerly of Terra Tek, Inc., and now with the Norwegian Geotechnical Institute (NGI) and Earth Technology, Inc., respectively, for rock characterization, instrument installation, and data analysis.

GENERAL DESCRIPTION

The Lucky Friday Mine (fig. 2) is located in the Coeur d'Alene Mining District in Idaho's "panhandle" region, approximately 95 miles east of Spokane, WA. The ore mined is silver-lead-zinc averaging about 18 tr oz of silver per short ton. Stoping is taking place as deep as the 5,100-ft level, with development occurring at the 5,300-ft level. The predominant mining method is nonmechanized overhand cut-and-fill using a breasting down or backstoping technique. A limited amount of undercut-and-fill stoping is also performed. In stopes, either rockbolts (fully resin-grouted, 7/8-in diam) or timber sets are used for support, depending upon ground conditions. In development headings, resin-grouted, Split Set,[4] or Swellex rockbolts with chain link fencing are used for ground support.

The rock mass consists of a series of steeply dipping, interbedded quartzites and quartzitic argillites of the St. Regis and Revett Formations. These beds range in thickness from inches to 3 or 4 ft, and range in composition from very hard and brittle, relatively pure quartzite to a soft argillitic quartzite. The beds are cut by semicontinuous joint surfaces on 12-in or less centers. Ground control problems include rock bursting and excessive closure. The No. 2 shaft, for example, exhibited large closures (in one case in excess of 1 ft in 1 month) (*9*) which resulted in extensive shaft set repair.

The Silver shaft (nominal 20-ft diam) is located some 1,000 ft west of the No. 2 shaft. Conventional drill-and-blast practices using handheld sinkers and a cactus grab rotary boom mucker mounted on the bottom of the Galloway work deck were employed during sinking. Preliminary support of the wall rock was provided by 5-ft Split Set bolts and chain link fence carried to within 4 ft of the working face. The liner, nominally specified by the contractor at 1-ft thickness, was carried 20 to 30 ft behind the face and advanced in 15-ft lengths. The heading was advanced by benching the north and south halves of the shaft at an average rate of 10 ft/d, with a record 1-month advance of 473 ft.

[4]Reference to specific products does not imply endorsement by the Bureau of Mines.

ROCK MASS CHARACTERIZATION

At each of the four test sites, a basic geologic map was prepared. In addition, the Norwegian Geotechnical Institute (NGI) Q-system (*2*) of rock mass characterization was employed to provide an estimate of rock mass properties.

Three significant geologic features that can have significant effects on the mechanical response of the rock mass are evident in the shaft: (1) Distinct, continuous bedding surfaces, (2) two sets of semicontinuous cross joints, and (3) shear zones that may or may not be conformable with bedding surfaces. The bedding represents a distinct set of parallel, continuous features. The spacing of the bedding planes averages about 0.5 to 1.5 ft at all horizons, with occasional thick (2 ft) or very thin (<6 in) beds. The strike of the bedding is consistent from level to level, averaging N 40° to 60° W with dips varying from about 60° to 80° SW. The bedding planes are cut by two sets of semicontinuous cross joints, which create a blocky appearance of the shaft walls. The first set strikes approximately S 70° to 90° W, dipping at 60° to 70° N, and has a spacing of about 6 in and a mean length of 10 to 20 in. The second set strikes 0° to 10° W, dipping 60° E to 80° W, and has similar spacing and length. Thus, there are three distinct discontinuities; however, only bedding is continuous over extended lengths.

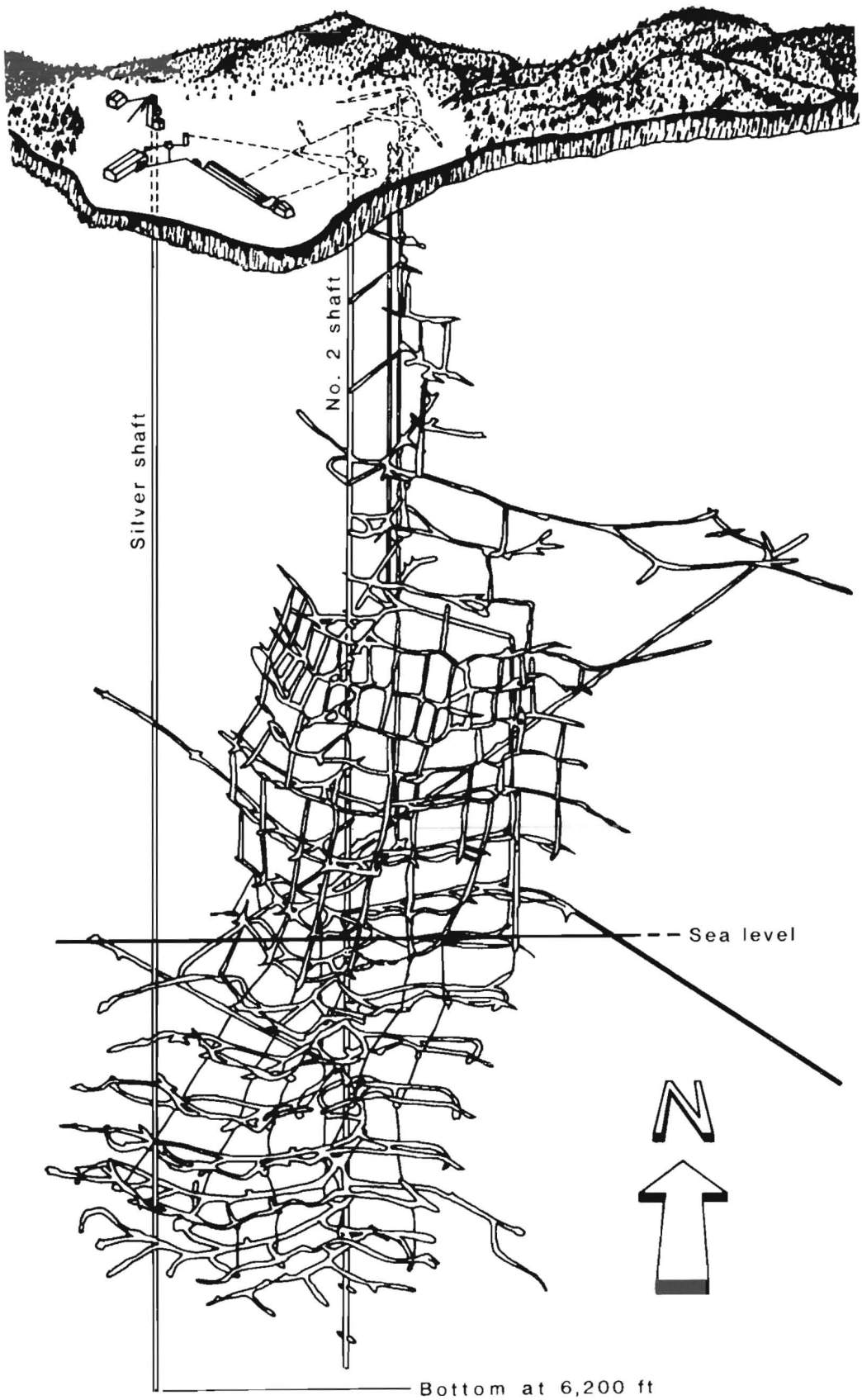

Figure 2.—Lucky Friday Mine and existing shafts and workings.

A rock mass classification was performed at each level as a means of estimating the engineering properties. The in situ deformation modulus was estimated with the NGI Q-system. The relation of the Q-value as well as the Council for Scientific and Industrial Research (CSIR) rock mass rating (RMR) system (*5*) to deformation modulus is shown in figure 3. The Q-classification is estimated from the rock quality designation (RQD), number of joint sets, the ratio of rock stress to strength, and the degree of weathering of the weakest set. In this case, the Q-value ranges from approximately 2 for the argillitic zone of thin beds to 10 to 15 for the massive quartzites. The modulus of deformation estimates for the rock mass vary distinctly with orientation because of the direction and intensity of jointing. The estimated values are summarized in table 1. These values reflect the orientation and distribution of fractures in directions perpendicular and parallel to the bedding structure. Further detail on each classification, Q-ratings, level geology, and rock strength is presented in appendix A.

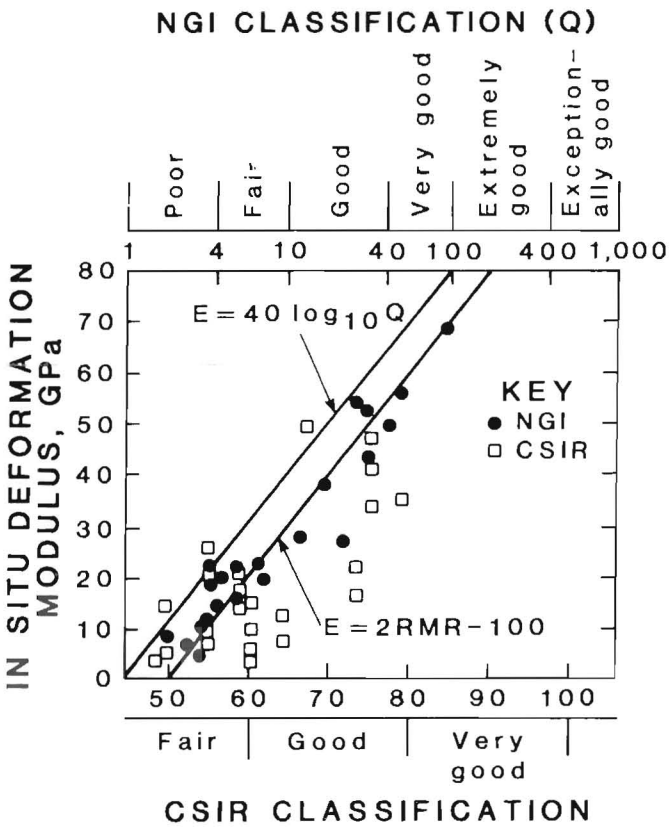

Figure 3.—Estimation of in situ modulus of deformation from Norwegian Geotechnical Institute (NGI) and Council for Scientific and Industrial Research (CSIR) classification methods.

TABLE 1.—Range of estimated quarzite deformation moduli from all test site, million pounds per square inch

Comments	Best quality	Heavily jointed
Parallel to bedding	6.0	3.0
Perpendicular to bedding	1.5	.5

In situ stress measurements have been performed at several locations in the Coeur d'Alene Mining District over the past 20 yr (*4, 11*). The general expressions for the in situ stress are

$$\sigma_v = 500 + 1.03\ d, \quad (1)$$

$$\sigma_{h1} = 707 + 1.37\ d, \quad (2)$$

and $$\sigma_{h2} = 530 + 1.05\ d, \quad (3)$$

where σ_v = vertical stress, psi,

σ_{h1} = maximum horizontal stress, psi,

σ_{h2} = minimum horizontal stress, psi,

and d = depth below surface, ft.

These data were used to project the magnitude and direction of the stresses at each of the test sites (table 2). The district-wide data show highly consistent directions of the maximum horizontal stress at N 45° to N 65° W, with a ratio of maximum to minimum horizontal stresses of 1.4.

TABLE 2.—Estimated vertical and horizontal principal stresses for all test sites, million pounds per square inch

Depth of test site, ft	Vetical stress	Horizontal stress	
		Maximum	Minimum
2,414	3,200	4,000	2,800
4,063	4,800	6,600	4,600
5,191	5,900	8,300	5,700
5,955	6,600	9,400	6,500

INSTRUMENTATION

The goal for in situ measurement was to monitor (1) rock and liner displacement, (2) liner stress change, and (3) liner strain. The instruments used for these measurements included multiple-position borehole extensometers (MPBX's) with grouted or hydraulic anchors, concrete pressure cells (PC's), embedment strain gauges (SG's), connecting signal cable, and a junction box (J-box). Surface equipment consisted of a data receiver and microcomputer with magnetic tape storage. All of the instruments and J-boxes were preassembled and sealed prior to

transport down the shaft. The goal was to produce a totally sealed, remotely accessed, environmentally secure package with no electronic or mechanical components exposed once the system left the shaft collar.

The MPBX's consisted of a reference head containing 2- to 4-in-range linear potentiometers, anchor assemblies, and stainless steel anchor extension rods. The 9-in-diam, mercury-filled PC's were precast into 12- by 12- by 4-in mortar briquettes and calibrated to 1,500 psi. This procedure negates effects of water migration to the stainless steel surface and initiates a positive output at low pressures.

The embedment SG's were cast into 3- by 6-in concrete cylinders with the bridge completion located in the encapsulation. The PC's were packaged individually and the SG's prewired into an array. All instrument cables were sealed with watertight Mil-Spec plugs attached to flexible conduit.

The J-box used was a NEMA IV, stainless steel 2- by 4-ft by 8-in-deep box containing two 16-channel Micromux data telemetry modules, power supply and terminal strips, and signal conditioning. This box was located in a manway or station within 200 ft of the instruments. The 32 channels of binary coded demical (BCD) integers, from 0 to 999 per channel, were multiplexed in frequency modulated pulses and transmitted serially in ASCII format up the shaft. Two shielded, twisted, 16-gauge wire pairs in self-supporting jacketed cables connected the two transmitters at each test site to the receiver station at the surface. The receiver stored the data, which were then available to a desktop computer or telephone modem.

The data acquisition system was designed to be simple and rugged. The on-site data processing system consisted of an HP85 desktop computer and pen plotter. Data acquisition software was used to convert raw data to engineering units. Raw and converted data were stored on magnetic tape, and could be plotted at the mine site. A paper tape printout of converted engineering values of each scan was also available. Data were sent via modem to a mainframe computer at the Bureau's Spokane (WA) Research Center where further data filing, manipulation, and plotting were performed. A detailed description of this instrumentation system has been published (*18*).

INSTALLATION

Based on preliminary studies, it was anticipated that the rock mass and support would respond to (1) excavation, (2) orientation (both with respect to geology and in situ stresses), and (3) radial distance from the shaft wall. The installation was designed to optimize the data based on this anticipated response and yet conduct the experiment under the constraints of time and budget. If the rock were elastic and homogeneous, the maximum radial displacement would occur in line with the maximum compression. However, it has been seen that, in most instances in the Coeur d'Alene mining district (with the exception of areas of high stress concentration), the geologic structure controls the location and direction of maximum displacement. This is particularly true when interbedded zones of hard, massive quartzites and squeezing argillites are encountered and maximum displacements occur perpendicular to the bedding. Therefore, extensometers were generally oriented with respect to the bedding in order to minimize the difficulty of data analysis.

Figure 4 is based on preliminary mapping and shows a plan view at each test site with instrument locations and orientations as well as the general rock structure and profile. The exact orientation of the MPBX holes is listed in appendix A.

Concrete PC's were used to determine stress distribution within the liner. To determine the optimum orientation of the PC's, the stress distribution in a circular ring subjected to external compression was examined. It was seen that the tangential stress in the liner was a much more sensitive indicator of external load than radial stress. Four PC's, placed at 90° intervals about the shaft circumference, were oriented to monitor tangential stress changes.

Strain in the liner was monitored with the concrete embedment SG's used at the 4,063-, 5,191-, and 5,955-ft-depth test sites. They were placed at 45° intervals and were oriented to measure tangential strain. Thermistors were also installed at the 2,414- and 4,063-ft-depth sites to determine the temperature distribution in the concrete and rock (see appendix B).

The installation sequence required about 2 days and followed a similar procedure at each test site. Installation was scheduled during downtime and holidays as much as possible to minimize interference with shaft sinking. Geologic mapping was followed by locating and drilling MPBX holes. In general, about 4 to 6 ft of muck was left on the bottom; this, coupled with the 3- to 4-ft height required to collar the hole, meant that the MPBX's were located approximately one shaft radius from the actual face. Small dogholes were blasted at each hole location so that the protective blockout over the MPBX head could be recessed flush with the shaft walls. Figure 5 shows an MPBX installed parallel to beds with the MPBX head in the doghole. Installation of the PC's and SG's occurred at

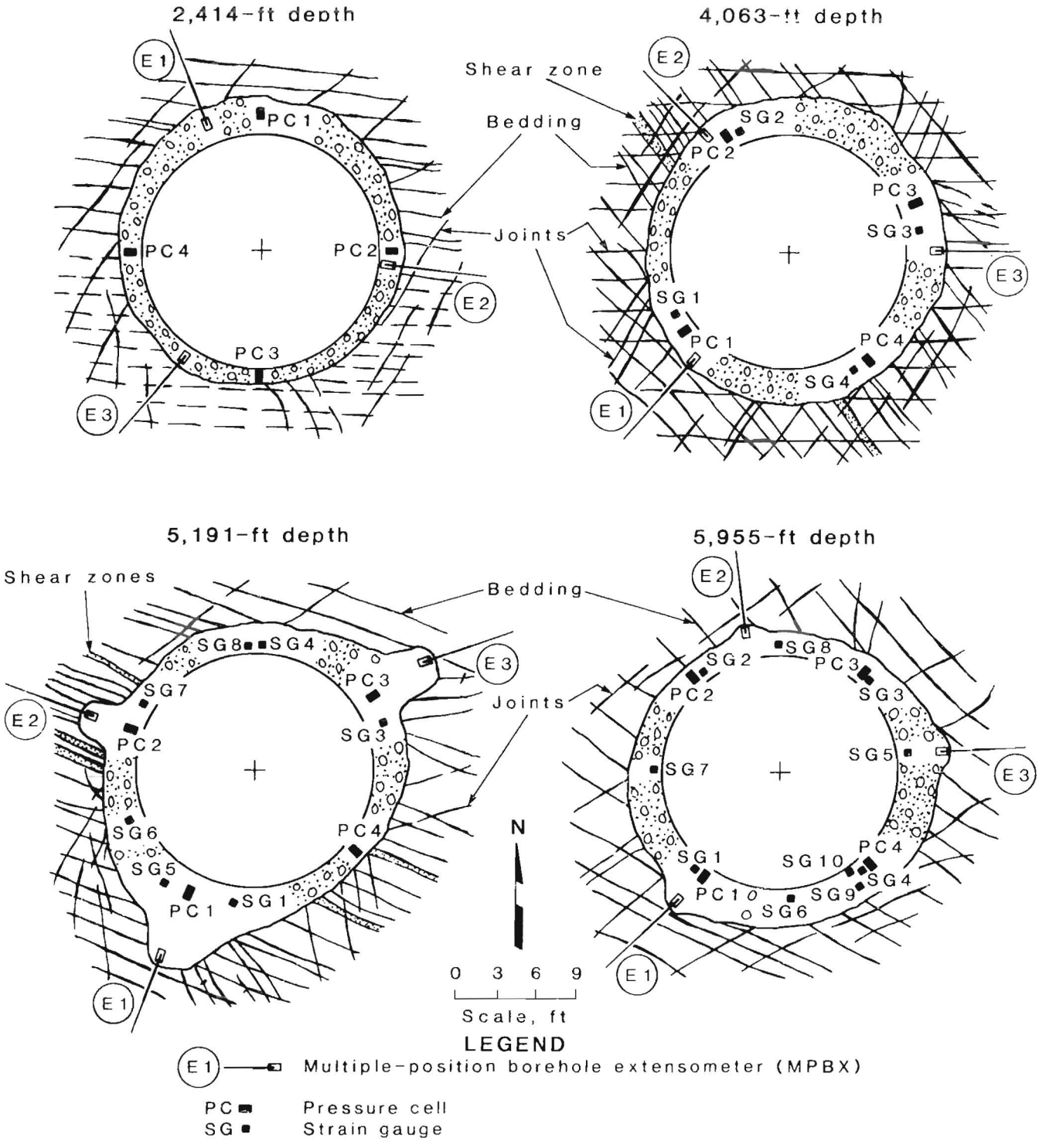

Figure 4.—Shaft test sites and instrument location, orientation, and rock profile.

Figure 5.—MPBX E2 instrument head recessed flush with shaft wall.

the same shaft depth once the concrete forms reached that level. Figure 6 shows a section through the shaft and the four test sites. Table 3 summarizes these installation activities and the time required for each installation.

The installations at the 2,414- and 4,063-ft depth sites followed a somewhat different approach. The concrete was carried to the shaft bottom and the MPBX blockouts brought out flush with the forms. The PC's and SG's were installed at the same time as the MPBX's. This afforded the necessary protection for the cables after sinking recommenced. However, this was not favored for the installations at the 5,191- and 5,955-ft depths because it was too disruptive of the normal sinking cycle. Figure 7 shows the PC and SG briquettes being installed in the fresh concrete in the kerb ring.

TABLE 3.—Installation date and time for various instrumentation activities, hours

Activity	2,414-ft depth, 4/23/81	4,063-ft depth, 9/10/81	5,191-ft depth, 4/26/82	5,955-ft depth, 2/17/83	Average[1]
Locate MPBX holes and perform geologic mapping	2.5	2	4	2	2
Drill holes	12	[2]21	[3]22	[3,4]22	19
Install MPBX's	10	[5]20	7	[6]8	9
Install PC's and SG's	3	4	3	3	3

[1]Does not include downtime for shaft repair, maintenance, etc.; average total was 33 h.
[2]Hoist down.
[3]Includes dogholes.
[4]Drill repair.
[5]Kerb ring interference.
[6]Hydraulic anchor plus grouting.

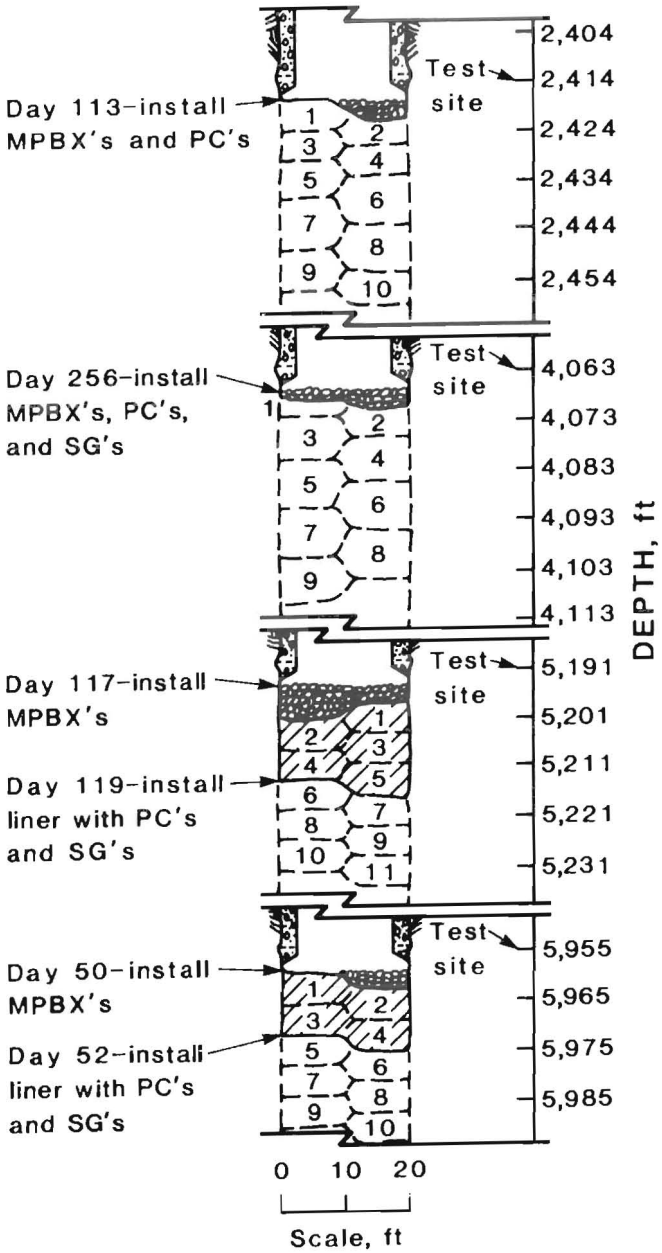

Figure 6.—Vertical profile of four test sites and installation and excavation schedule.

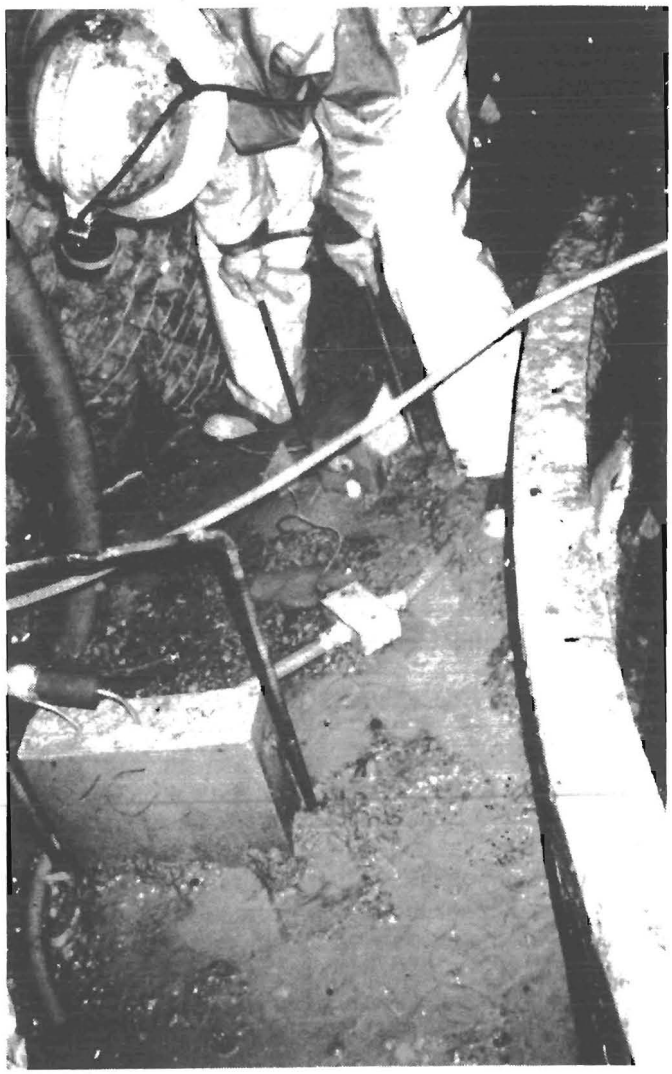

Figure 7.—Pressure cell and strain gauge briquettes being installed in kerb ring.

RESULTS

Initial data processing provided plots of the measured parameters over any desired time interval. Displacement plots show movement of individual anchor points relative to the most stable anchor, which was generally the deepest anchor at a depth of 55 to 60 ft. The complete set of data in appendix C shows displacement versus elapsed time (days since installation) of 5, 10, and 30 days, and tables of maximum displacement and liner pressure and strain. The plots presented in the text have been selected to illustrate the major response factors.

Instrument responses including those extraneous to the effect of ground movement, such as temperature differentials, rigid inclusion effects, concrete and grout shrinkage, and modulus contrast and variation with time, are also reflected in the initial data plots. For example, one major extraneous response was the effect of temperature and shrinkage of the liner and grout column in the MPBX holes. An initial displacement excursion of up to 0.1 in over the first 8 to 16 h following installation is evident in the MPBX plots. In most cases, this effect stabilized prior to initial zero readings. Another suspected source of error was a mechanical stick-slip type behavior on some of the deepest anchor extensions, particularly those exhibiting large movements. This resulted in an erroneous sense of movement in the referenced data. This malfunction was resolved by rereferencing to a more stable, shallower anchor position and is so noted in the plots.

ROCK MASS DISPLACEMENT

The maximum displacement on all instruments was measured at the collar of the borehole on the shaft wall. At the 2,414- and 4,063-ft-depth sites, where the MPBX heads were located in the concrete liner, the indicated movement was actually less than that shown by the shallow anchors located in the rock. Figure 8 shows 5-day shaft wall displacements over a specific interval of elapsed time at each test site for each MPBX location, during which face advance was equivalent to approximately two to three shaft diameters. The exact blasting times are indicated by arrows. Appendix D lists the actual blast schedule for each test site. With the exception of the 2,414-ft depth, the orientation of the MPBX's to bedding followed a consistent pattern, i.e., E1–normal, E2–parallel, and E3–45°. At the 2,414-ft depth, the instruments were located 120° apart, with one parallel (E2) and two at 45° (E1 and E3) to the bedding strike.

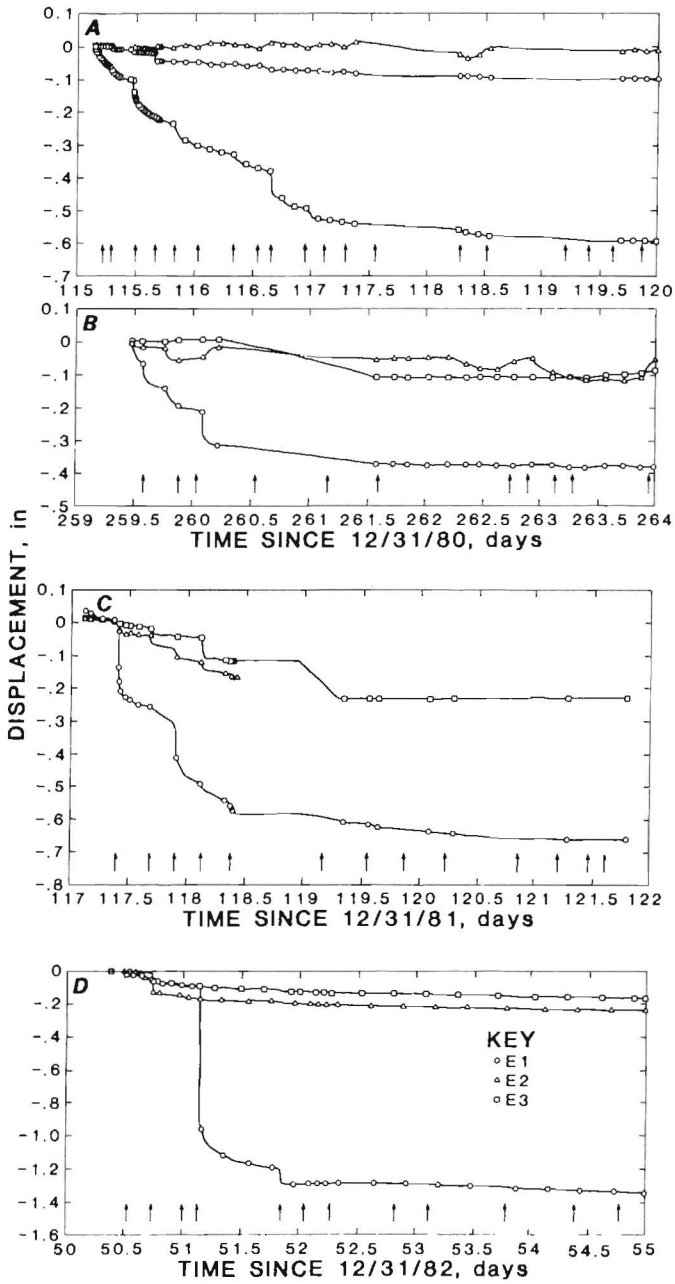

Figure 8.—Shaft wall displacements measured by MPBX E-1—E-3 over initial 5-day interval. *A*, 2,414-ft depth; *B*, 4,063-ft depth; *C*, 5,191-ft depth; *D*, 5,955-ft depth.

Displacement normal to bedding was several times greater than that measured 45° or parallel to the bedding. The ratio of maximum to minimum shaft wall displacement is 6:1 at the 2,414- and 5,955-ft depths and 3:1 at the other two depths. The high ratio at the 2,414- and 5,955-ft depths is probably the result of shear zones that crossed the MPBX holes at locations near the shaft wall (see appendix A for details).

Figure 9 shows shaft wall displacements for 30 days elapsed time at each test site. The displacement rate steadily decreased and was minimal after 10 to 12 drill-and-blast cycles, representing about 40 to 60 ft of shaft advance beyond the instrumented level. This decrease in displacement rate usually occurred within the first 5 days following installation. Again, at the 2,414- and 5,955-ft depths, normal to the bedding strike, greater time-dependent displacement was exhibited.

The instruments at all four test sites exhibited similarities in response. There was an instantaneous and discrete displacement jump immediately following each blast. Each instrument responded depending on its proximity to the bench being blasted and distance from it to the shaft bottom. Some instruments reflected a significant time-dependent component of displacement between blasts, particularly normal to the bedding, which in some cases almost equaled the instantaneous response. All of these response characteristics are illustrated in figure 10.

The installation at the 5,955-ft depth exhibited anomalous behavior, but was found to be due to secondary excavation of a loading pocket about 45 ft below the instruments (*3*). Displacement was reactivated as shaft excavation resumed, as seen in figure 9*D*, at about 11 days elapsed time. MPBX-E3, which was oriented roughly parallel (within 10°) of the longitudinal axis of the loading pocket, was most responsive. The additional increment of collar displacement due to loading pocket excavation and subsequent shaft sinking was almost 60 pct of the initial displacement levels at day 79. The displacement was also fairly deeprooted, as even the 15-ft anchor position showed additional movement (fig. C-15).

LINER STRESS AND STRAIN

The PC's and SG's were oriented to measure tangential stress near the neutral axis of the unreinforced liner. This location in the liner was selected to minimize the effects of liner bending on the measured stress. Figures 11 and 12 show the 5-day responses of the PC's and SG's, respectively. Times of individual blasts again are indicated

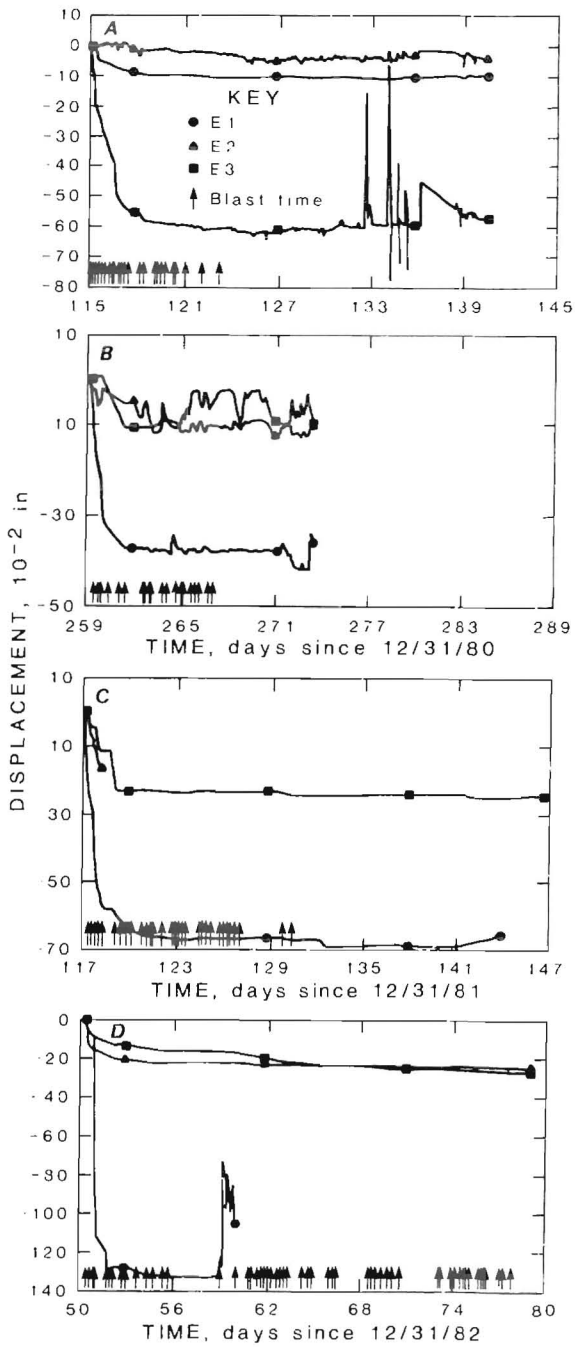

Figure 9.—Shaft wall displacements for 30 days' elapsed time. *A*, 2,414-ft depth; *B*, 4,063-ft depth; *C*, 5,191-ft depth; *D*, 5,955-ft depth.

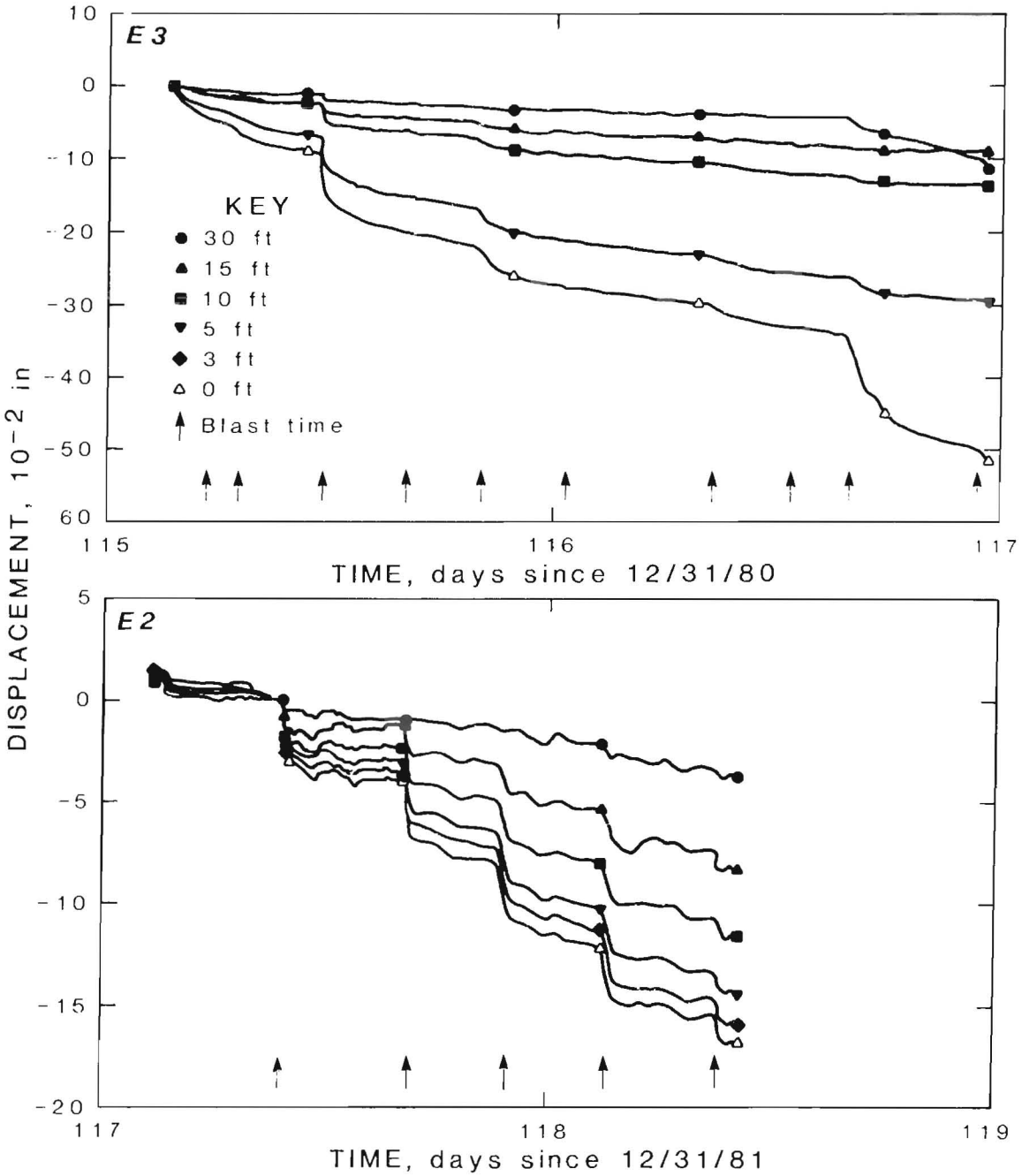

Figure 10.—Typical response characteristics at indicated hole depth for MPBX E3 at 2,414 ft for the first 10 blasts and MPBX E2 at 5,191 ft for the first 5 blasts.

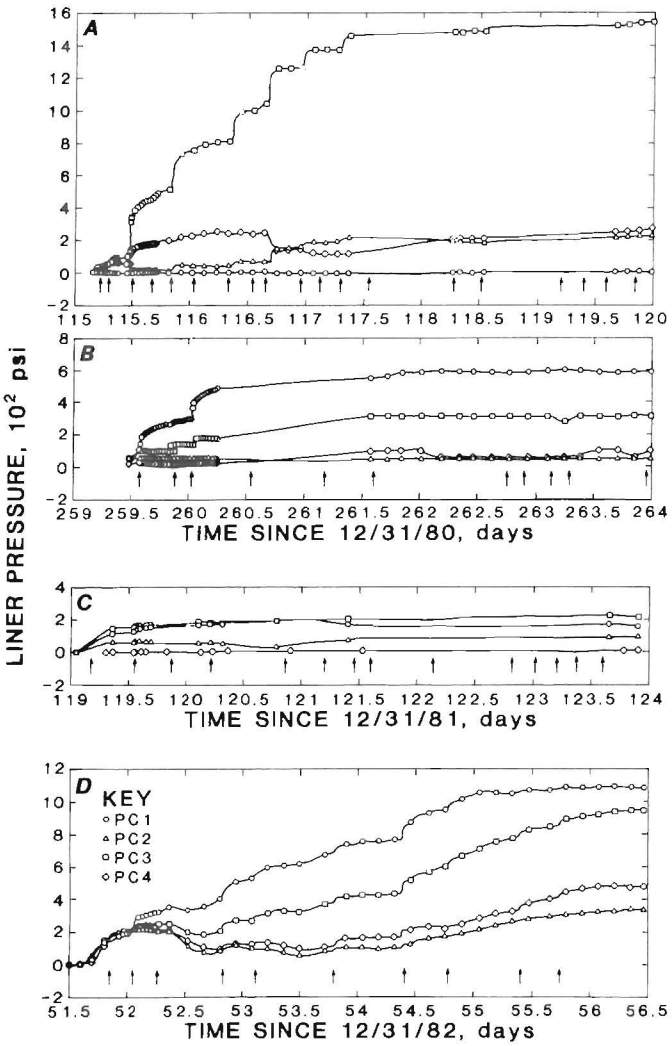

Figure 11.—Liner pressure developed over 5-day interval following installation. *A*, 2,414-ft depth; *B*, 4,063-ft depth; *C*, 5,191 ft depth; *D*, 5,955-ft depth.

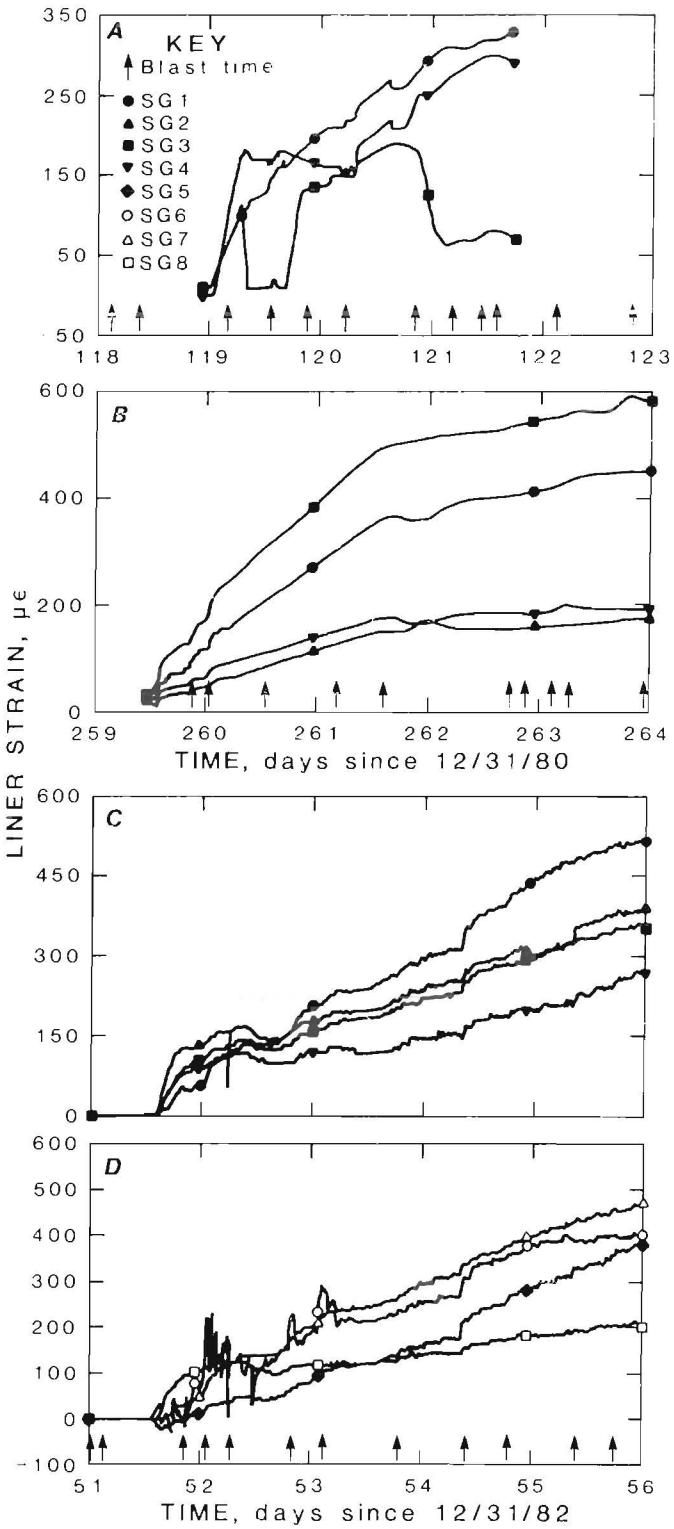

Figure 12.—Liner strain developed over 5-day interval following installation. *A*, 4,063-ft depth; *B*, 5,191-ft depth; *C-D*, 5,955-ft depth.

by arrows. For the 2,414- and 4,063-ft levels, the liner was installed to the shaft bottom. On the 5,191- and 5,955-ft levels, the liner was installed in the normal fashion, 18 to 20 ft above the shaft bottom. As with the movement of the shaft wall rock (as indicated by the MPBX's), the PC's and SG's indicated discrete jumps at each blast. In addition, there was a significant creep component between blasts, due largely to curing of the concrete, particularly during the first 24 h following installation.

The tangential stress measured parallel with the bedding (southwest and northeast quadrants) was consistently larger than that measured normal to the bedding. In addition, the stress on the footwall (southwest) side of the shaft was generally larger than that measured on the hanging wall (northeast) side. The maximum tangential stress ranged from less than 300 psi at the 5,191-ft depth to 1,100 psi on the 5,955-ft depth and nearly 1,600 psi on the 2,414-ft depth. Minimum tangential liner stresses (the northwest-southeast quadrants) ranged from less than 100 psi on the 5,191-ft depth to about 500 psi at the 5,955-ft depth.

The SG's, installed adjacent to the PC's at the last three test sites, generally tracked the PC's performance, although they exhibited a slightly more dominant creep behavior. Their magnitudes generally supported the PC results, particularly on the last installation at the 5,955-ft depth.

Maximum tangential strains measured at the 4,063-, 5,191-, and 5,955-ft test sites were 650, 400, and 600 $\mu\epsilon$, respectively, all measured in either the southwest or northeast quadrants. Minimum strains were 200, 200, and 300 $\mu\epsilon$, respectively. Again, as with the MPBX's, the liner stress and strain at the 5,955-ft depth increased substantially as a result of excavation of a loading pocket at the 6,000-ft depth. This effect can be seen in figures 11*D*, 12*C*, and 12*D* and has been previously discussed in detail (*3*). Liner stress and strain rates decreased, indicating equilibrium after about 12 drill-and-blast cycles (face advance beyond the test site equivalent to two to three shaft diameters).

DATA ANALYSIS

The primary purpose of the data analysis given here is to examine models of rock-support interaction to determine their applicability in the design of deep mine shafts in highly stressed ground. Much attention has been given to the interaction between the rock mass and tunnel lining during the construction process. The estimation of concrete liner stresses in tunneling and shaft sinking is normally accomplished using analytical equations that account for the interaction of the rock mass and the support (*10*).

These analytical methods have been developed for a variety of isotropic constitutive laws, including elastic and elastoplastic behavior and hydrostatic rock stress in two dimensions. This analysis has recently been extended to unequal biaxial field stresses (*8*). The three-dimensional effects of face advance have also been examined numerically (*16*), resulting in the development of support delay attenuation factors (fig. 13). These factors are used to reduce, or "attenuate," calculated values when comparing them with measured values that reflect only a portion of the total displacement that has occurred. These methods are generally used in practice to provide a conservative estimate of induced liner stress for the assumption of plane strain. The liner design (primarily thickness) or installation method (delay behind the face) can then be weighed against the possibilities of ground instability or increased liner cost.

The actual field problem in shaft sinking varies from the preceding idealized case in several respects. First, the liner is generally placed at least one shaft diameter behind the face. At this point, most of the elastic rock mass displacement has already occurred (*1, 10, 17*). For a poured concrete liner, the concrete also remains green for some time as face advance continues. At an advance rate of 6 to 10 ft/d, which is standard in shaft sinking practice, the face can advance two shaft diameters in less than 1 week, and thus displacement equilibrium can occur before maximum concrete strength is reached. This effect is offset to a certain extent by the use of additives that promote high early strength.

Second, the radial stresses exerted on the liner can be highly nonuniform as a result of geologic structural control of rock mass displacements. The two assumptions implicit in the rock-support interaction concept–radial symmetry and a continuum representing rock mass behavior–place limits on the ability to model response where structural features are of importance. The induced radial tangential

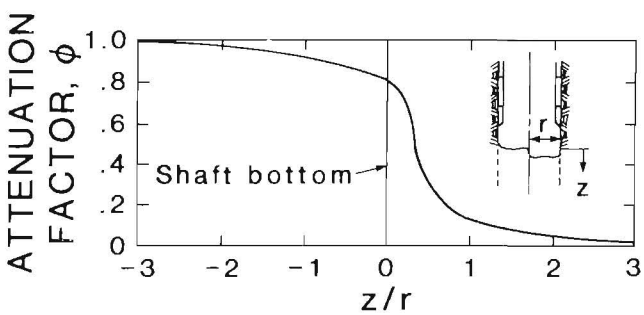

Figure 13.—Effects of support delay showing attenuation factor ϕ, the factor used to reduce calculated values so they agree with measured values, as a function of ratio between measurement distance above shaft bottom z and shaft radius r.

stresses in cast-in-place concrete liners in a jointed rock mass under unequal field stresses have been examined. In one study (*13*), the distinct-element method was used to model the rock mass, and was coupled to a matrix structural analysis approach for the concrete liner. Interface shear and normal stiffness were varied to simulate effects such as liner backpacking.

Displacement of the rock mass about the Silver shaft is largely a function of bedding plane orientation where maximum displacements occur normal to the bedding. Since there were no analytical methods available to the Bureau for describing the rock-support interaction resulting from the anisotropic displacements indicated, the approach taken to data analysis was twofold:

1. Examination of the mechanisms by which the rock mass structure apparently controls the radial displacements.

2. Examination of the use of existing rock-support interaction approaches for bounding the range of measured liner stresses.

This methodology is somewhat empirical since existing rock-support interaction solutions are not well suited for this problem. However, suitable engineering approaches for preliminary specification of liner dimensions are possible. A methodology that provides for a conservative support design under the conditions of nonuniform external loading is considered a reasonable and prudent approach.

DISPLACEMENTS

The rock mass displacements recorded at all four test sites indicated a high degree of consistency. In all cases, a transverse isotropy was indicated, with maximum displacement normal to the strike of the bedding. Some general observations can be made from the series of displacement plots given in figures 8 and 9. Components located at 45° and parallel to bedding indicate a near-elastic response and can be fit reasonably well using the Kirsch solution and a deformation modulus within the range given in table 1. The normal displacement component, however, indicated large, nonelastic deformations that were confined to about one-half to one shaft radius into the wall rock. At greater distances, the displacements converged for all anchors once equilibrium was established. The yielding observed here could be a general continuum response or the result of isolated discrete block motion into the shaft caused by sliding along existing fracture surfaces.

Initial studies performed shortly after the installation were based upon rock-support interaction models (*7*). The measured displacements were compared to analytical solutions for the displacements based upon elastic or elastoplastic rock mass behavior. However, none of these solutions adequately explained the displacements because of the effect of anisotropy, which are very different to model.

ROCK MASS AS A TRANSVERSELY ISOTROPIC ELASTIC BODY

An initial transversely isotropic elastic analysis was conducted to determine the adequacy of this material model in explaining the displacements. As a test case, the data from the 5,955-ft-depth test site were used for comparative purposes. A boundary-element approach was used to model the excavation in two dimensions and the axes of elastic anisotropy were assumed to coincide with the orientation of the bedding. The deformation modulus parallel to bedding (E_x) was varied from 3 to 6.0 million psi and that normal to the bedding from 0.5 to 1.5 million psi, as derived from the rock mass characterization discussed earlier. A transversely isotropic body requires three additional elastic constants: the cross-shear modulus, G_{xy}, and the Poisson's ratios, ν_{xy} and ν_{yx}. Although G_{xy} is an independent property, the following formula for determining the shear modulus based on rock laboratory testing has been suggested (*12*):

$$G_{XY} = \frac{E_X E_Y}{E_Y (1 + 2\nu) + E_X} , \qquad (4)$$

where $\nu = \nu_{XY} = \nu_{YX}$.

Using equation 4, the cross-shear modulus was estimated to be in the range of 0.5 to 1.2 million psi using a Poisson's ratio of 0.2. Implicit in this analysis is the assumption that the bedding dips at 90° to the horizontal plane. As the bedding actually dips at 60° to 80°, there is an error in this assumption. A series of parameter runs were made in which the material properties were varied and displacements determined. In all cases, an attenuation factor from figure 13 was applied to reduce the two-dimensional displacement calculations to account for the effect of face advance and support delay. The results indicated a reasonable agreement with the near-elastic response to MPBX's E2 and E3, as was expected. However, the agreement with the collar and 5-ft anchor displacements for MPBX E1 was seriously in error.

One complicating factor in this analysis was the presence of a shear zone striking roughly perpendicular to MPBX E1 approximately 2 ft into the MPBX hole. This shear zone had a fairly thick band of clay gouge and obviously caused additional radial displacement at the first two anchor points. Comparison of the transversely isotropic solution to data from the other instrumented horizons yielded somewhat better results, but the analyses were still seriously in error.

The results of this analysis indicated three points of importance:

1. The response of the MPBX's parallel and at 45° to bedding strike was reasonably elastic.

2. The displacement response normal to bedding strike was nonelastic.

3. The depth of the yield zone was about 10 ft or less (one shaft radius) as indicated by return to elastic response at this distance.

DIRECTIONAL PLASTICITY MODEL

To account for the nonelastic response in the normal direction, a directional plasticity-slip plane approach was examined. A so-called ubiquitous joint model was incorporated into the explicit finite-difference program, NESSI (*6*). In this model, the rock mass is assumed to be a continuum whose material response is governed by a series of weak planes that exist everywhere within the mass. The rock mass is numerically characterized by joint orientation and material properties. The joint plane constitutive behavior is given by the standard Mohr-Coulomb yield criterion, which can include dilation if desired.

During the calculations, an initial trial elastic-stress increment is computed at each time step. The stresses perpendicular and parallel to the joint direction are determined and compared to the yield surface. If the material has yielded, i.e., if the stress state falls outside the failure envelope, the shearing stress on the joint plane is reduced to keep the stress state on the yield surface. The corrected stresses are then rotated back to the global frame and cycling to equilibrium is continued in the same manner. At each time step, the stress state of each zone can be examined.

A parameter study was conducted using this model for a single set of joints coincident with the bedding surfaces. The material joint parameters, including friction angle and cohesion, were varied while the direction and magnitude of the in situ stresses remained constant. The results are illustrated in figure 14 where the predicted and actual displacements versus radial distance are plotted at equilibrium for the three MPBX locations at each test site. An attenuation factor has been applied to the two-dimensional calculations to account for face advance.

The model reasonably reproduces the measured data from all four sites. The model is able to produce the important feature of a large displacement contrast between the direction normal and parallel to structure. An approximately elastic response is seen at the parallel and 45° MPBX (E-2, E-3) locations.

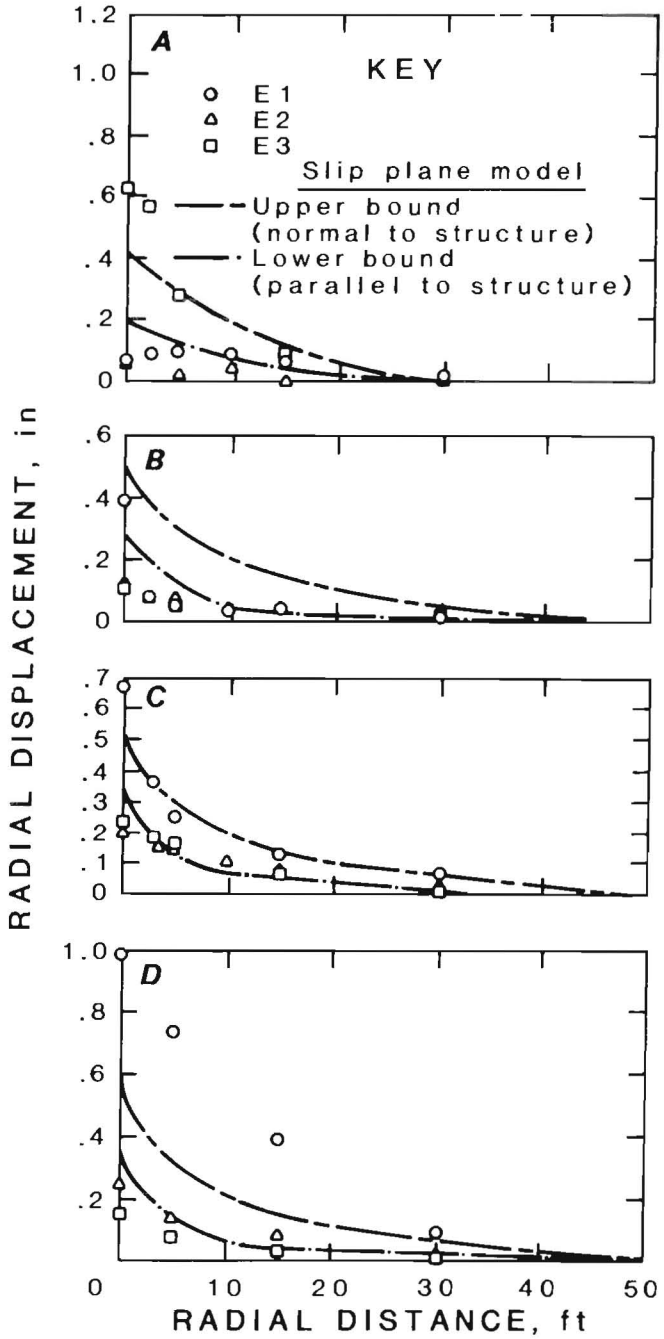

Figure 14.—Measured versus calculated radial displacement plotted as a function of radial distance for each MPBX location (E-1—E-3) at each site. *A*, 2,414-ft depth; *B*, 4,063-ft depth; *C*, 5,191-ft depth; *D*, 5,955-ft depth.

The poorest correlation occurs at the collar anchors on the perpendicular MPBX's (E1) from the 2,414- and 5,955-ft depths and can be related to geologic conditions unique to both test sites. At the 2,414-ft depth, a conformable contact between a soft, thinly bedded argillite and a hard, medium-bedded quartzite roughly separate the northern and southern halves of the shaft. The collar of MPBX E3 was located in the soft argillite, which was unconsolidated enough to be removed fairly easily with a pickax. At the 5,955-ft depth, a clay gouge zone was encountered 2 ft into the hole at being drilled for MPBX E1. In both of these cases, the ratio of maximum (normal) to minimum (parallel and 45°) displacement was approximately 6:1, whereas it was about 3:1 at the 4,063- and 5,191-ft test site depths.

LINER STRESS

The primary goal of the analysis of liner stresses is to provide a reasonable engineering estimate of the stresses as a function of the in situ stress state and distance behind the face when the liner is installed. At the present time, an analytic rock-support interaction solution for a directionally yielding rock mass under unequal biaxial stresses is not known to exist. Therefore, a directly analogous approach to the liner stress analysis as was taken for the displacements cannot be performed. The goal of providing an engineering estimate of liner response can still be accomplished using existing methods. The solution for a thick ring embedded in an elastic rock mass with a non-slipping interface and unequal biaxial in situ stresses is used to bound the measured liner stresses for the range of estimated in situ moduli and liner thicknesses.

The problem of a thick elastic ring embedded in an elastic rock mass with a no-slip interface was examined. The geometry of this problem is illustrated in figure 15. Excavation and support installation are assumed to occur simultaneously and rock reinforcement, such as a Split Set or grouted bolts, is not considered. The solution for liner tangential stresses is presented as a function consisting of components proportional to the hydrostatic, P°, and deviatoric, S°, stress components:

$$\sigma_t = P^\circ S_h(r) + S^\circ S_d(r) \cos 2\theta, \quad b < r < a. \qquad (5)$$

where σ_t = tangential liner stress,

P°, S° = hydrostatic and deviatoric stress components,

$S_h(r)$, $S_d(r)$ = dimensionless stress functions,

and θ = angular measurement from the X axis.

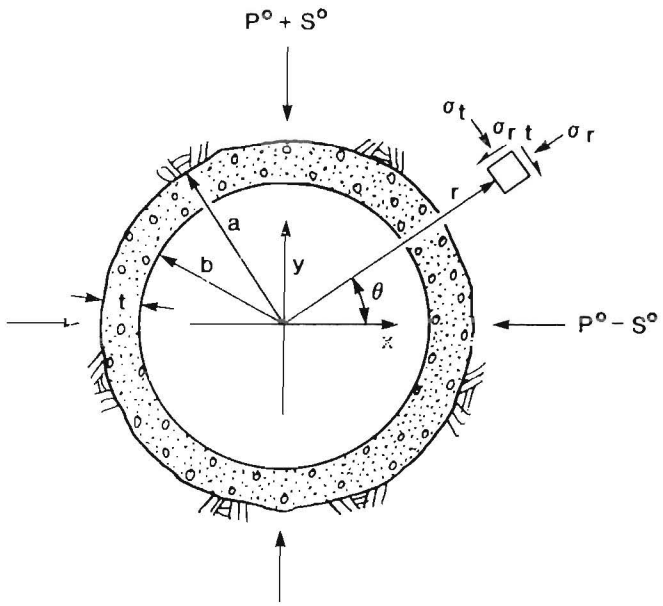

Figure 15.—Geometry of concrete liner modeled as a thick elastic ring embedded in elastic rock mass with no-slip interface.

The two stress functions, $S_h(r)$ and $S_d(r)$, depend upon five dimensionless parameters: $\lambda = G_1/G_2$, the ratio of the shear moduli of the liner to rock; $\rho = b/a$, the ratio of the inner to outer radius of the liner; t/a, the ratio of the liner thickness to outer radius; and ν_1 and ν_2, the Poisson's ratios of the liner and rock, respectively. The deviatoric stress portion is dependent upon the type of rock-liner interface condition.

This analysis does not consider support delay, and thus an overestimation of load is predicted using this equation. An attenuation factor is used to account for support delay. During the first two installations, the liner was placed approximately one radius behind the working face. Because of the operational difficulties of kerb ring installation and the high induced tangential stress in the liner (see figure 11*A*), the decision was made to drop the liner back to approximately 20 ft behind the face on the final two installations. The resulting attenuation factors of 0.3 and 0.1 were applied to stress predictions for the 2,414- and 4,063-ft depths and the 5,191- and 5,955-ft depths, respectively.

A parameter study was conducted to compare measured tangential liner stress to stress calculated by equation 5. Two parameters have the most important effect on tangential stress: the shear modulus, ratio, λ, and the ratio of liner thickness to outer radius, t/a (table 4). The effects of the λ variation are fairly obvious; however, the parameters t and a can cause opposite variation in σ_t; e.g., a

TABLE 4. - Computed values of $\sigma_t(max)/\sigma_t(min)$ for various t/a and G_1/G_2 ratios

Ratio of liner thickness to outer shaft radius (t/a)	Ratio of shear moduli of liner to rock (G_1/G_2)					
	0.6		0.8		1	
	σ_t(max)	σ_t(min)	σ_t(max)	σ_t(min)	σ_t(max)	σ_t(min)
0.15	1.17	0.55	1.48	0.72	1.76	0.88
0.20	1.15	.57	1.44	.73	1.69	.88
0.25	1.13	.59	1.39	.74	1.62	.88

NOTE.—The value of σ_t must be multiplied by ϕP° obtain the actual value of the tangential stress.

thicker liner attracts higher support load because of increased stiffness, but the resulting thrust is transmitted by a larger cross sectional area. The fact that σ_t(max) decreases with increasing t/a reflects primarily the effect of large bending moments in the structure. The variation in thickness, however, has little effect on the stresses for low values of λ.

In the actual field case, the thickness of the liner varied with angular position about the shaft because of underbreak and/or overbreak. This variation in thickness was significant and ranged from 9 to 55 in (nominal design thickness of 12 in) at the four test sites. For the calculations presented here, the liner thickness was varied over that range at that particular depth, whereas the value of λ varied from 1 to 0.25, corresponding to the moduli estimates presented earlier. The assumption was also made that the concrete deformation modulus was constant at 2 million psi, based on the high early strength additives used in the concrete.

The results of the study are presented in figure 16. The tangential stress is plotted as a function of angle from the deviatoric stress direction. Each plot represents a separate test site and shows the calculated and actual field measurements for the cases of λ = 1 to λ = 0.25 and for the range of liner thicknesses at that depth.

Several conclusions can be drawn from these plots. The field measurements indicate the same maximum and minimum locations as predicted by the no-slip formulation; the maximum stress occurs at ±90° from the principal horizontal stress direction. Also, the field data are bounded by the moduli contrasts given.

The data from the 4,063- and 5,191-ft depths match well for a λ = 0.25. For the 2,414- and 5,955-ft depths, the σ_t(min) corresponds well to the lower bound of λ = 0.25, but the σ_t(max) is anomalous, corresponding to a λ of 1. These were also the depths where the anomolously high displacements occurred normal to the bedding.

It is possible that nonuniform loading of the liner from rock mass structural variations resulted in larger induced stresses, as was previously shown (*13*). A larger component of deviatoric in situ stress would also result in more rapid change in the tangential component with angular distance around the shaft, but this would be expected on the basis of data from the other two test sites (4,063- and 5,191-ft depths) where a smooth variation was seen.

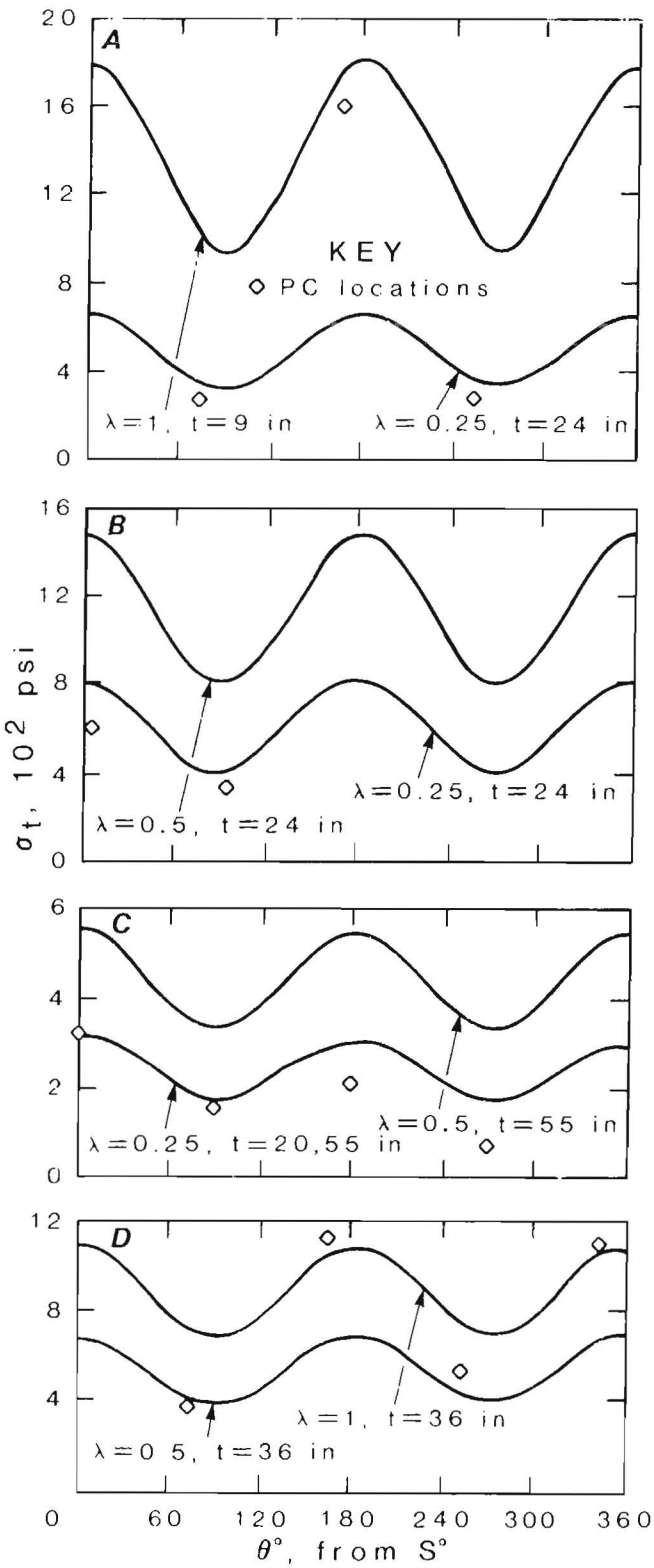

Figure 16.—Measured versus calculated tangential liner stress at each site (shear modulus ratio, λ; liner thickness, t). *A*, 2,414-ft depth; *B*, 4,063-ft depth; *C*, 5,191-ft depth; *D*, 5,955-ft depth.

Finally, λ = 0.25 corresponds to a rock mass deformation modulus of 8 million psi, assuming a Young's modulus for concrete of 2 million psi. Whereas this is possible, it is likely that the deformation modulus for the concrete is, instead, in the range of 1 to 1.5 million psi over the time these measurements were taken (i.e., about 10 days).

In summary, the above mentioned model equation 5 for predicting liner stresses accounts for the general variation of the tangential stress and can be shown to bound the field data for the field moduli range estimated using the Q-system. This model can be considered a reasonably conservative engineering estimate and is sufficient in the present case because extensive yielding of the rock mass did not occur.

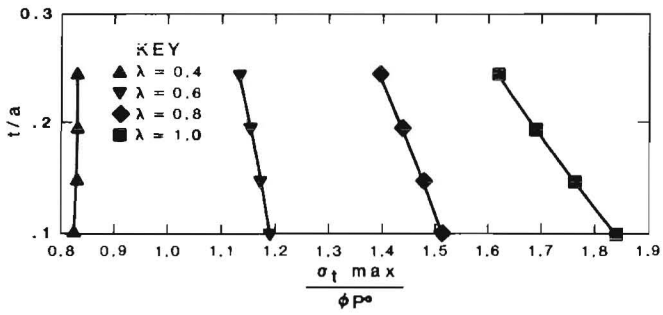

Figure 17.—Effect of normalized liner thickness t/a to normalized tangential stress $\sigma_t(max)/\phi P^\circ$ for various shear modulus ratios (λ).

IMPLICATIONS FOR SHAFT DESIGN

The primary design criteria of interest are (1) what minimum nominal liner thickness can be used and (2) how far behind the face can the liner be carried while maintaining a reasonable factor of safety against liner failure. A parameter study was conducted using the solution of equation 5 and various values of support delay, liner thickness, and concrete-to-rock mass shear modulus ratio (λ). A general plot illustrating the relation of t/a to the normalized average tangential stress at its maximum position ($\sigma_t(max)/\phi P^\circ$) for various values of the shear modulus ratio is given in figure 17. For a given hydrostatic stress component, P°, support delay factor, ϕ (from fig. 13), and shear modulus ratio, λ, the required liner thickness can be calculated. Thus, for general design purposes, the value of $\sigma_t(max)$ can be calculated and compared to the concrete liner strength (assuming that no tensile stress exists) with any desirable factor of safety.

For the specific case of the Silver shaft, plots have been developed that illustrate the required support delay in terms of shaft radius as a function of depth for various ratios of t/a and λ (fig. 18). These plots assume a 4,000-psi compressive strength concrete and a factor of safety of 2.0. The bounding value of λ = 1.0 shows that for a support delay of two shaft radii, the maximum shaft depth before liner failure is about 8,000 ft. During construction, the shaft bottom reached 6,200 ft with one diameter delay with no liner stability problems.

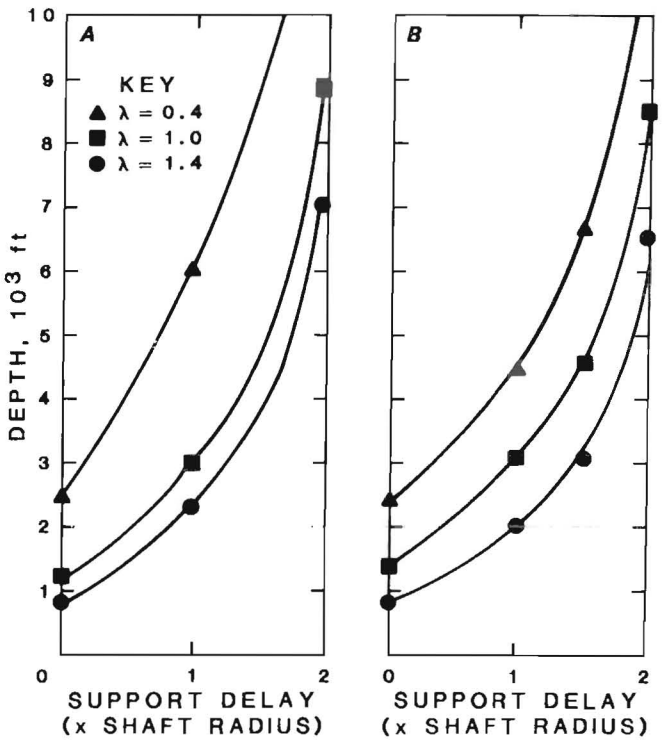

Figure 18.—Required support delay as a function of shaft depth for various shear modulus ratios (λ). *A*, t/a = 0.2; *B*, t/a = 0.1.

CONCLUSIONS

There are many factors affecting the structural stability, and thus design, of a deep mine shaft. Variable factors include the size, shape, and orientation of the shaft, the type and dimension of support, and the time lag between excavation and support installation. Fixed conditions include the magnitude, direction, and ratio of in situ stresses, geologic environment, and rock mass properties. Of crucial importance to the present investigation is a preliminary evaluation of the in situ stress field and physical properties of the rock mass.

Measurements during construction of a deep shaft have shown that the effect of rock mass anisotropy is considerable. A variety of numerical and analytical models have been used to bracket the measured response and thus characterize the in situ conditions. A methodology for liner specification has been proposed in which the deformation moduli of the rock mass are estimated from rock characterization. An elastic no-slip rock-support interaction approach was used with estimated moduli to bracket the measured liner response. Based on a combination of observational, analytical, and empirical approaches, overall behavior of the rock mass and support system in a deep mine shaft has been determined. Application of these methods to future shaft construction and repair will provide deep mine operators with needed information for proper design and stability evaluations.

REFERENCES

1. Abel, J. F., Jr., J. E. Dowis, and D. P. Richards. Concrete Shaft Lining Design. Paper in 20th U.S. Symposium on Rock Mechanics. Dep. Petroleum Eng., Univ. TX, Austin, TX, 1979, pp. 627-640.

2. Barton, N., F. Losit, R. Lien, and J. Lunde. Application of Q-System in Design Decisions Concerning Dimensions and Appropriate Support for Underground Installations. Subsurface Space, Pergamon, 1980, pp. 553-561.

3. Beus, M. J., and M. P. Board. Field Measurement of Rock Displacement and Support Pressure at the 5,955-ft Level During Sinking of a Deep Circular Shaft in Northern Idaho. BuMines RI 8909, 1984, 11 pp.

4. Beus, M. J., and S. S. M. Chan. Shaft Design in the Coeur d'Alene Mining District, Idaho—Results of In Situ Stress and Physical Property Measurements. BuMines RI 8435, 1980, 39 pp.

5. Bieniawski, Z. T. Determining Rock Mass Deformability: Experience From Case Histories. Int. J. Rock Mech. Min. Sci. and Geomech. Abstr., v. 15, 1978, pp. 237-247.

6. Cundall, P. A. User's Manual and Report on NESSI, Version 1.145. Shell Res. KSEPL, Rijswijk, Netherlands, 1983, 70 pp.

7. Daemen, J. J. K. Tunnel Support Loading Caused by Rock Failure. Ph.D. Thesis, Univ. MN, Minneapolis, MN, 1975, 445 pp.

8. Detournay, E. Two-Dimensional Elastoplastic Analysis of a Deep Cylindrical Tunnel Under Non-Hydrostatic Loading. Ph.D. Thesis, Univ. MN, Minneapolis, MN, 1983, 133 pp.

9. Gooch, A. E., and J. P Conway. Field Measurements and Corresponding Finite-Element Analysis of Closure During Shaft Sinking at the Lucky Friday Mine. BuMines RI 8193, 1976, 19 pp.

10. Hoek, E., and E. T. Brown. Underground Excavations in Rock. Inst. of Min. and Metall. (London), 1980, pp. 244-286.

11. Langstaff, J. Hecla's Seismic Detection System. Paper in Site Characterization: 17th U.S. Symposium on Rock Mechanics (Snowbird, UT). Univ. UT, Salt Lake City, UT, 1976, pp. 3 A7-1—3 A7-20.

12. Lekhnitskii, I. Theory of Elasticity of an Anisotropic Elastic Body. Holden-Day, 1981, 430 pp.

13. Lorig, L. A Hybrid Computational Scheme for Excavation and Support Design in Jointed Media. Ph.D. Thesis, Univ. MN, Minneapolis, MN, 1984, 237 pp.

14. McKinstry, B. A. Sinking the Silver Shaft. Paper in Proceedings, 1983 Rapid Excavation and Tunneling Conference, ed. by H. Sutcliffe and J. W. Wilson (Chicago, IL, June 12-16, 1983). AIME and ASCE, v. 1, Chicago, 1983, pp. 493-512.

15. Miller, R. P. Engineering Classification and Index Properties for Intact Rock. Ph.D. Thesis, Univ. IL, Urbana, IL, 1965, 332 pp.

16. Schwartz, C. W., and H. H. Einstein. Inspired Designs for Tunnel Supports: Volume 1—Simplified Analysis for Ground-Structure Interaction in Tunneling. U.S. Dep. Transportation Rep. DOT-TSC-UMT7-80-27.I, 1980, 450 pp.

17. Terzaghi, K., and L. Richart. Stresses in Rocks Around Cavities. Geotechnique, v. 2, No. 1, 1952, pp. 57-75.

18. Whyatt, J. K., and E. Hardin. Microcomputer-Based Instrumentation System for Monitoring Ground Support in a Deep Mine Shaft. BuMines IC 9062, 1985, 88 pp.

APPENDIX A.–ENGINEERING GEOLOGY

Numerous laboratory measurements of the physical properties of Coeur d'Alene Mining District rocks have been made (*4*).[1] Table A-1 summarizes typical mean values of Poisson's ratios and Young's Elastic moduli determined at various mines in the Revett and St. Regis Formations.

The initial instrumentation station in the Silver shaft was at or near the contact of the St. Regis and Revett Formations. The lower stations were all within the Revett quartzites. The St. Regis Formation is characterized by argillitic quartzites with interbedded argillites, while the Revett Formation consists primarily of hard, medium-to-massive, bedded, clean quartzites.

There is also a wide variation in strength properties of the quartzites. The factor that most affects the strength is discontinuities, which range from microfractures to large-scale weakness planes. Of greatest interest here is that most laboratory samples behave in a highly linear manner prior to failure. Table A-2 shows typical laboratory determined strength parameters for the Revett and St. Regis Formations.

However, values pertinent to the present study are more appropriately determined by methods that integrate the major geologic features of the rock mass. Therefore, joint strike and dip readings, rock mass classification values (Q- and RMR-systems), and data on Schmidt hammer rebound for unconfined compressive strengths were obtained. Little time was available for mapping the geology of the shaft at the instrument locations because of scheduling and conditions that were far from ideal.

[1]Italic numbers in parentheses refer to items in the list of references preceding this appendix.

TABLE A-1.–Elastic parameters for Revett and St. Regis Formations

Formation and mine	Young's modules, 10^6 psi	Poisson's ratio
Revett:		
Lucky Friday ...	8.10 ±0.75	0.25 ±0.07
Star	9.26 ±1.48	.29 ± .075
St. Regis:		
Calladay	9.57 ± .28	.205± .048
Sunshine	10.54 ±1.39	.26 ± .070

TABLE A-2.–Strength parameters for Revett and St. Regis Formations

Formation and mine	Uniaxial compressive strength, psi	Tensile strength, psi	Cohesion, psi	Angle of friction, deg
Revett:				
Lucky Friday	44,916±5,530	1,710±446	NA	NA
Star	20,613±1,237	3,496±321	NA	NA
St. Regis:				
Calladay	18,275±4,993	2,200±292	2,836	52
Sunshine	23,036±3,513	2,619±690	3,300	50

NA Not available.

2,414-ft Test Site

Marginally different bedding orientations in the argillite and quartzite were observed with mean strike and dip orientations of 93° and 80° S and 59° and 75° S, respectively. The approximate north-south split between the quartzite and argillite is across the east-west diameter of the shaft. Wedge-shaped overbreak features in the quartzite, shown in figure A-1 on the northeast side of the shaft, indicate the presence of at least two additional sets of joints.

The lithology and joint structure revealed by mapping suggest strongly anisotropic deformability. Estimates of Q-values obtained from joint mapping in the shaft ranged from approximately 2 in the argillite to 8 in the quartzite, suggesting upper-bound values of deformation moduli (E) in the range of 1.7 to 5.1 psi, respectively. The estimates of upper-bound deformation moduli obtained from these Q-values may imply the possible ranges at this depth (table A-3).

An obvious reason for the broad range of E-values generally experienced is the orientation of loading relative to major joint sets. In the case of the shaft, a larger value would be expected in a loading (or unloading) direction parallel to the bedding strike, i.e, approximately east-west. A lower value would obviously be expected perpendicular to bedding (north-south). Any joint shearing mechanism (due to diagonal loading) would be likely to give the lowest values of all. Thus, from a geological engineering viewpoint, E-values in the various MPBX directions might be crudely estimated from the above considerations as follows: MPBX E2 (NNW), approximately perpendicular to bedding (quartzite), ≈3.2 million psi; MPBX E3 (E), approximately parallel to bedding (quartzite), ≈5.2 million psi; and MPBX E1 (SSW), approximately 20° inclination to bedding (argillite), ≈0.5 million psi.

TABLE A-3.—Estimates for in situ deformation modulus at 2,414-ft depth, million pounds per square inch

	Argillite	Quartzite
Emax	1.7	5.1
Emean	1.1	3.2
Emin	.4	1.3

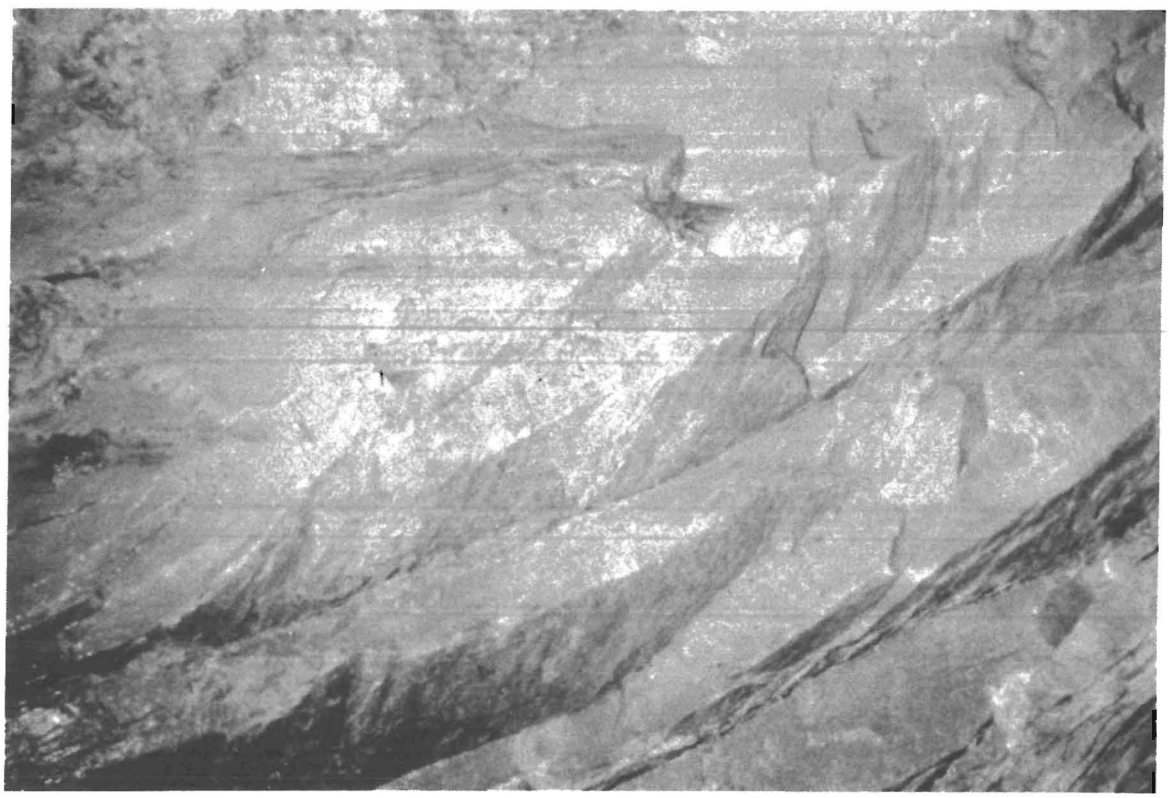

Figure A-1.—Wedge-shaped overbreak features on northeast side of shaft.

Laboratory tests have indicated a good correlation between the Schmidt L-hammer rebound number (R), the rock density, and the laboratory-scale unconfined compression strength (*15*). The following two sets of values were recorded in the shaft on the sound (nondrummy) areas of rock: North side (quartzite) 55, 57, 60, 35, 50, 62, 34, 25, and 50, mean of 48; south side (argillite) 47, 44, 45, 35, 32, and 27, mean of 38.

Assuming rock densities of 180 lb/ft^3 and 165 lb/ft^3 for quartzite and argillite, respectively, these mean values suggest laboratory-scale, unconfined compression strengths of approximately 22,860 psi and 10,700 psi, respectively. While these values have only a minor influence on rock mass strengths (because of jointing), they appear realistic for small, intact samples.

4,063-ft Test Site

The rock found at the second test site consists predominately of green-tan, thin-to-medium-thick, bedded, slightly argillaceous quartzite having sericite on the bedding surfaces. Thin beds of fine-grained, green argillite occur every few feet. A marked northwest-southeast-trending shear zone parallels the bedding. The shear zone contains approximately 5 to 15 cm of crushed quartzite and fine gouge (fig. A-2). Because of local undulations of the bedding, strike readings range from about N 40° to 60° W, with a southwesterly dip of about 56° to 64°. In general, the bedding joints are spaced 15 to 50 cm apart, but increase in number (5 to 15 cm apart) across the center of the shaft on either side of the shear zone. Two sets of less-continuous cross-joints intersect the bedding, giving the walls of the shaft a blocky appearance. Because of the dip of the beds and the combination of heavy blasting and high stress, there was considerable overbreak in the northeast side of the shaft.

The thin beds on either side of the shear zone have an average Q-value around 3 to 4, and an RMR-value of about 57. This suggests a mean deformation modulus of about 2 million psi, but a wide range is possible. It is not clear what influence the shear zone has in reducing this value. The crushed quartzite and gouge filling are probably transmitting normal stress in the range of 5,000 to 7,000 psi, which suggests the bedding zone will be

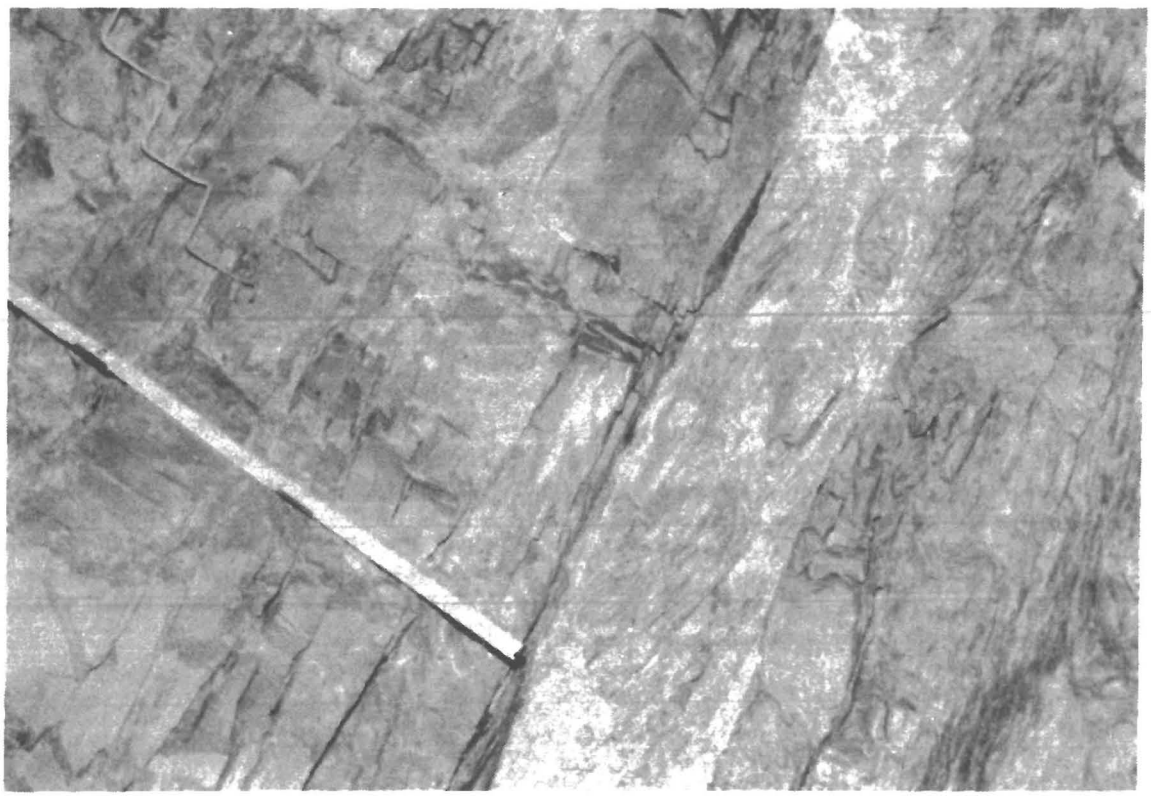

Figure A-2.—Northwest-southeast-trending shear zone containing crushed quartzite and fine gouge paralleling beds.

extremely stiff compared to a shear zone at the moderate depth.

The more massive quartzite on either side (southwest and northeast) of the zone of thin beds has a Q-value of about 10 to 15, suggesting a mean deformation modulus in the range of 4.3 to 5.7 million psi. Estimates for in situ deformation modulii are listed in table A-4. The rock mass deformation modulus estimated for each extensometer direction is shown in table A-5.

TABLE A-4.—Estimates for in situ deformation moduli at 4,063-ft depth, million pounds per square inch

	Best quartzite	Jointed zone
Emax	6.3	3.3
Emean	3.9	2
Emin	1.6	.8

TABLE A-5—Estimated moduli of deformation[1] at various extensometer orientations at four test sites, million pounds per square inch

Test site depth, ft	MPBX Hole	MPBX Orientation	Est modulus	Bedding orientation
2,414	E1	S 35° W	0.5	
	E2	N 25° W	3.2	N 80° W
	E3	S 85° E	5.2	
4,063	E1	S 45° W	1.6	
	E2	N 45° W	3.4	N 50° W
	E3	E-W	3.9	
[2]5,191	E1	S 23° W	1.2	
	E2	N 68° W	4.7	N 70° W
	E3	N 58° E	NA	
[2]5,955	E1	S 36° W	0.8 -1.6	
	E2	N 16° W	3.3 -6	N 65° W
	E3	N 79° E	NA	

NA Not available.
[1]Based on rock mass quality (Q) designation.
[2]Based on a 4,063-ft-depth analysis and similar geology for parallel and perpendicular directions.

5,191-ft Test Site

The rock type at this depth is predominately yellowish- to grayish-tan, medium-bedded quartzite. A greenish-tan, 0.5- to 1.5-ft thick, soft argillite was noted in the north wall. Bedding trends west-northwest to east-southeast, with a steep dip toward the southwest, quite consistent with the dip of the bedding at the previous instrument site. The principal bedding and joint orientations observed at the 5,191-ft depth had a strike value of N 65° to 75° W and a dip value of 64° to 76° SW.

The appearance of the bedding joints is shown in figure A-3. On the south side of the shaft, at the position of MPBX E1, the beds dip away from the observer, with a typical joint spacing of 12 to 18 in. On the north side of the shaft, the spacing is more typically 4 to 10 in. More marked secondary jointing makes the south side of the shaft appear more jointed than the north.

The east-west diameter of the shaft is characterized by more closely spaced bedding joints, particularly between two minor crushed zones, where the spacing is down to 1 to 2 in locally.

A classification of rock mass quality based on the Q-system is as follows:

$$Q \approx RQD/J_n \times J_r/J_a \times J_w/SRF$$

where RQD = rock quality designation, 75,

J_n = two joint sets plus random, ≈6,

J_r = rough, planar joint surfaces, ≈1.5,

J_a = unaltered joint surfaces, ≈1.0,

J_w = medium pressure water inflow, ≈0.66,

and SRF = mild rock burst, ≈8.

The resulting Q-value [(75/6) × (1.5/1.0) × (0.66/8)] is 1.5. As a result of slabbing and occasional bursting, the rock mass is classified in the poor category, with Q-values generally in the range 1 through 4.

The compressive strength of the rock at this level (laboratory-scale values) was estimated by means of a Schmidt L-hammer survey incorporating at least 20 tests. The following values were obtained: 42, 40, 45, 48, 40, 45, 46, 50, 54, 50, 56, 56, 50, 50, 48, 56, 44, 44, 42, 40, and 46.

The overall mean of 47 and the mean of the highest 10 results (52) suggest unconfined compression strengths approximately in the range of 18,850 to 24,650 psi. Table A-5 summarizes the estimated modulus values for the four test sites.

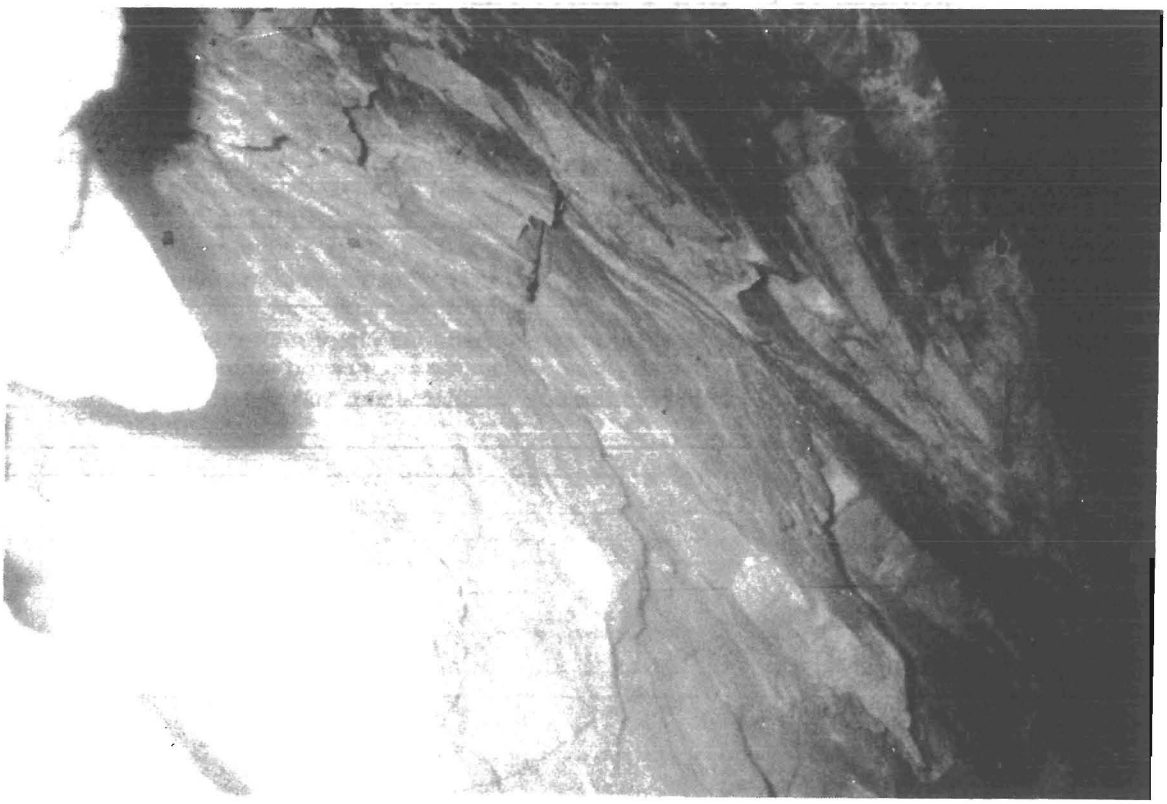

Figure A-3.—Bedding joints dipping toward observer with slickensides on exposed surface.

APPENDIX B.–ROCK AND CONCRETE TEMPERATURE

For the initial installation, two sets of thermistors were used, one set within the instruments in the liner, and one set along MPBX E1 with measurement points 5, 10, 15, and 20 ft back from the collar. A typical plot of the temperature as a function of time is shown in figure B-1. The pressure cell (PC) thermistors indicate that maximum curing temperature was reached within 15 h. The magnitude varied and depended on the localized thickness of the liner. For example, thermistor TPC 1 was located where the liner was nearly 3 ft thick and temperatures reached a maximum of about 51° C, whereas the liner at TPC 3 was only 9 in thick and resulted in a maximum temperature of about 42° C. After approximately 5 days, all thermistors were slowly approaching equilibrium of about 26° C.

The extensometer thermistors showed that a temperature gradient of less than 1° C existed between the 5- and 20-ft radial distances. The rock mass temperature increased by about 0.5° to 1° C because of the presence of the liner. The rock temperatures equilibrated at 27° C after approximately one-half day. In addition, the measurements indicated little, if any, thermal gradient in the shaft. One important result of the temperature measurements was that no temperature correction to the MPBX displacements was required.

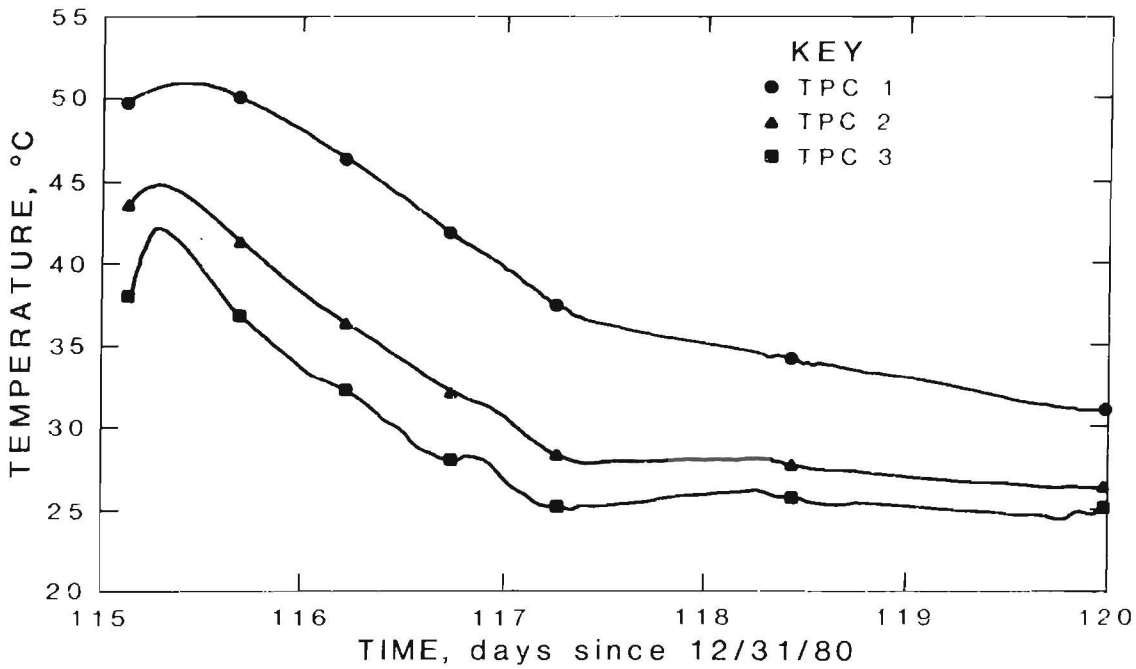

Figure B-1.–Temperature versus time for thermistors at PC 1, PC 2, and PC 3 for the first 5 days after installation at 2,414-ft depth.

APPENDIX C.–MAXIMUM DISPLACEMENTS, LINER PRESSURES, AND LINER STRAINS

TABLE C-1.–Maximum radial displacement from four test sites, inch

Instrument depth, ft	MPBX E1, normal	MPBX E2, parallel	MPBX E3, 45°
2,414	[1]0.620	0.050	[1]0.100
4,063	.375	[1].120	.096
5,191	.720	[1].190	.240
5,955	.880	.225	[2].250

[1]Argillite or argillitic shear zone.
[2]Displacement following loading pocket excavation at 6,000 ft was 1.5 in.

TABLE C-2.–Maximum liner stress from four test sites, pounds per square inch

Instrument depth, ft	PC 1	PC 2	PC 3	PC 4
2,414[1]	Neg	250	1,550	250
4,063	580	Neg	320	80
5,191	250	250	[2]375	125
5,955	1,100	400	1,050	500
([3])	1,850	850	2,050	1,250

Neg Negligible; insufficient contact, leakage, or improper orientation.
[1]Oriented north, south, east, and west.
[2]Oriented 225° from PC 1.
[3]Increase in pressure because of loading pocket excavation at 6,000 ft.

TABLE C-3.–Maximum liner strain from four test sites, microinch per inch

Instrument	Depth, ft				([1])
	2,414	4,063	5,191	5,955	
SG 1	NAp	600	580	575	850
SG 2	NAp	200	([2])	460	500
SG 3	NAp	700	200	440	1,100
SG 4	NAp	200	300	325	800
SG 5	NAp	NAp	([2])	450	1,250
SG 6	NAp	NAp	[3]200	450	750
SG 7	NAp	NAp	([2])	520	950
SG 8	NAp	NAp	([2])	250	200
SG 9	NAp	NAp	NAp	325	800
SG 10	NAp	NAp	NAp	375	900

NAp Not applicable.
[1]Increase in strain because of loading pocket excavation at 6,000 ft.
[2]Malfunctioning instrument.
[3]Unencapsulated.

TABLE C-4.–Liner stress and strain at selected stages of shaft sinking following instrumentation at 5,955 ft

Activity	Stress, psi				Strain, μin/in							
	PC 1	PC 2	PC 3	PC 4	SG 1	SG 2	SG 3	SG 4	SG 5	SG 6	SG 7	SG 8
Sink shaft from 5,977 to 6,000 ft, 7 days elapsed time.	1,100	350	1,000	500	560	450	425	325	450	450	525	250
Excavate loading pocket at 6,000 ft 14 days elapsed time.	1,400	500	1,700	900	700	550	600	550	800	550	675	350
Sink shaft from 6,000 to 6,070 ft, 27 days elapsed time.	1,750	650	2,000	1,100	900	650	800	650	1,050	650	900	425
Complete shaft to 6,200 ft, 66 days elapsed time.	[1]950	800	[1]1,750	1,200	1,000	725	975	800	1,275	775	1,050	500
No activity, 298 days elapsed time.	650	750	650	1,100	900	900	1,200	825	1,400	([2])	1,050	475

[1]Possible malfunction of pressure cells.
[2]Malfunction of strain gauges.

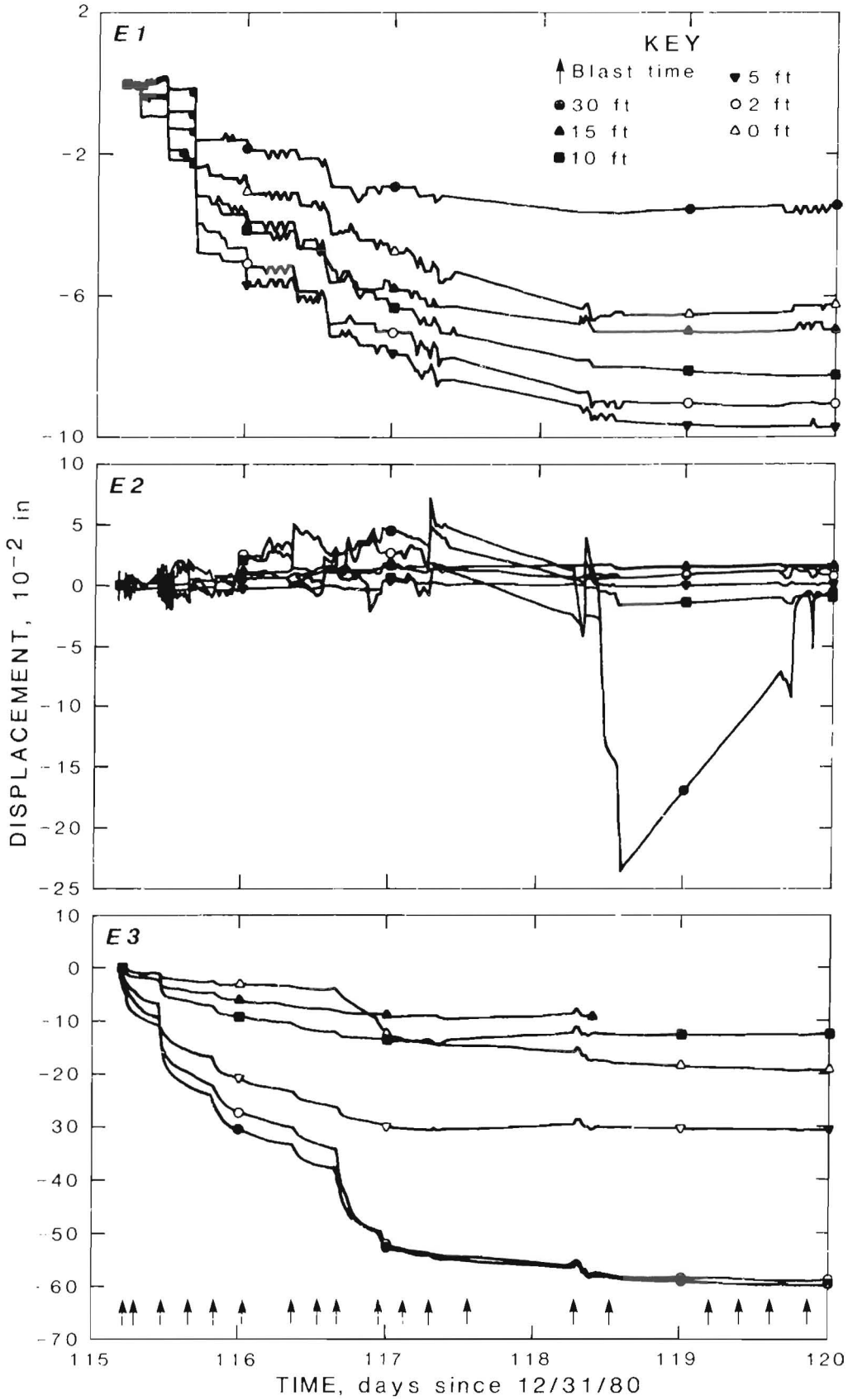

Figure C-1.—2,414-ft depth—5-day displacement at each MPBX location *(E-1—E-3)*.

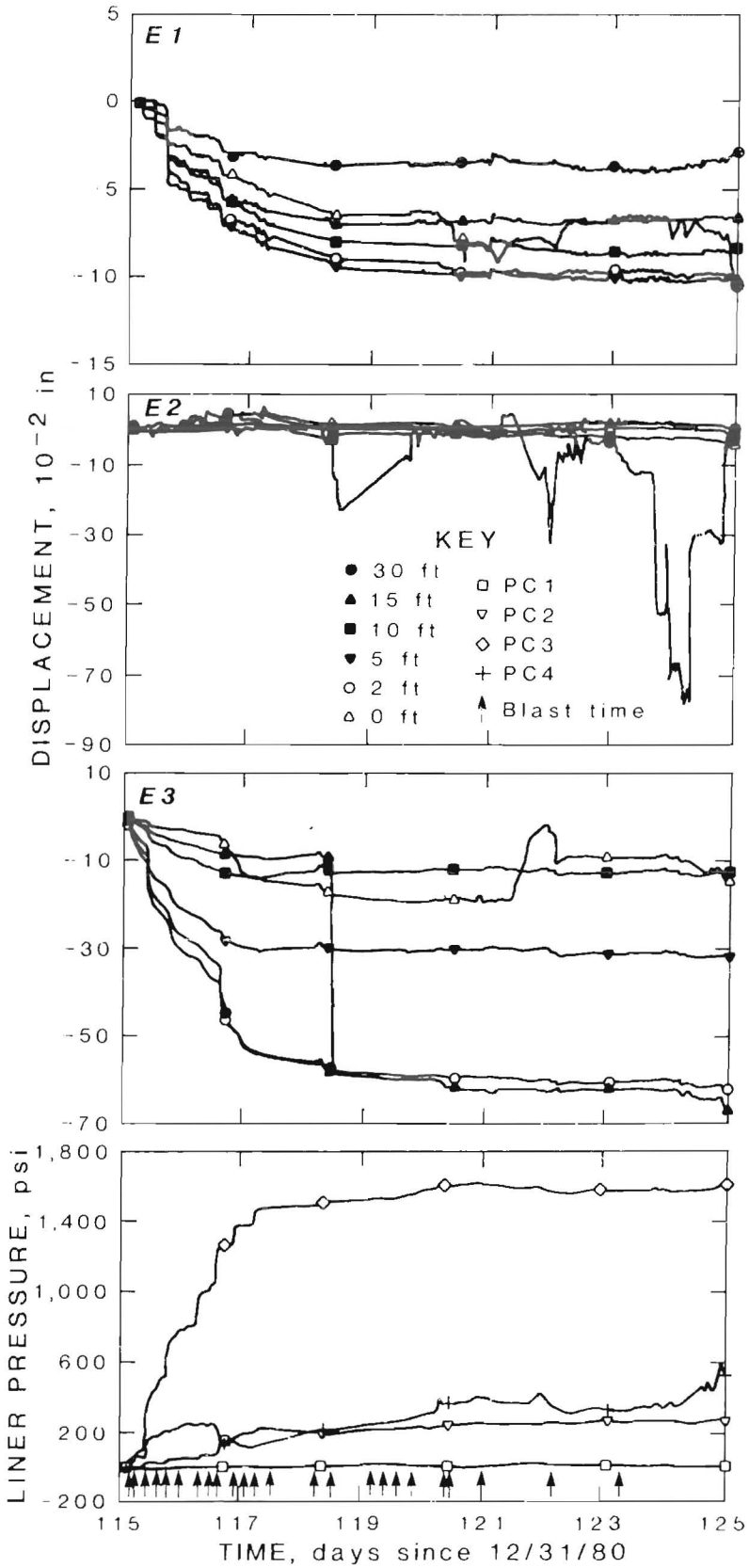

Figure C-2.—2,414-ft depth—10-day displacement and liner stress at each MPBX location *(E-1—E-3)*.

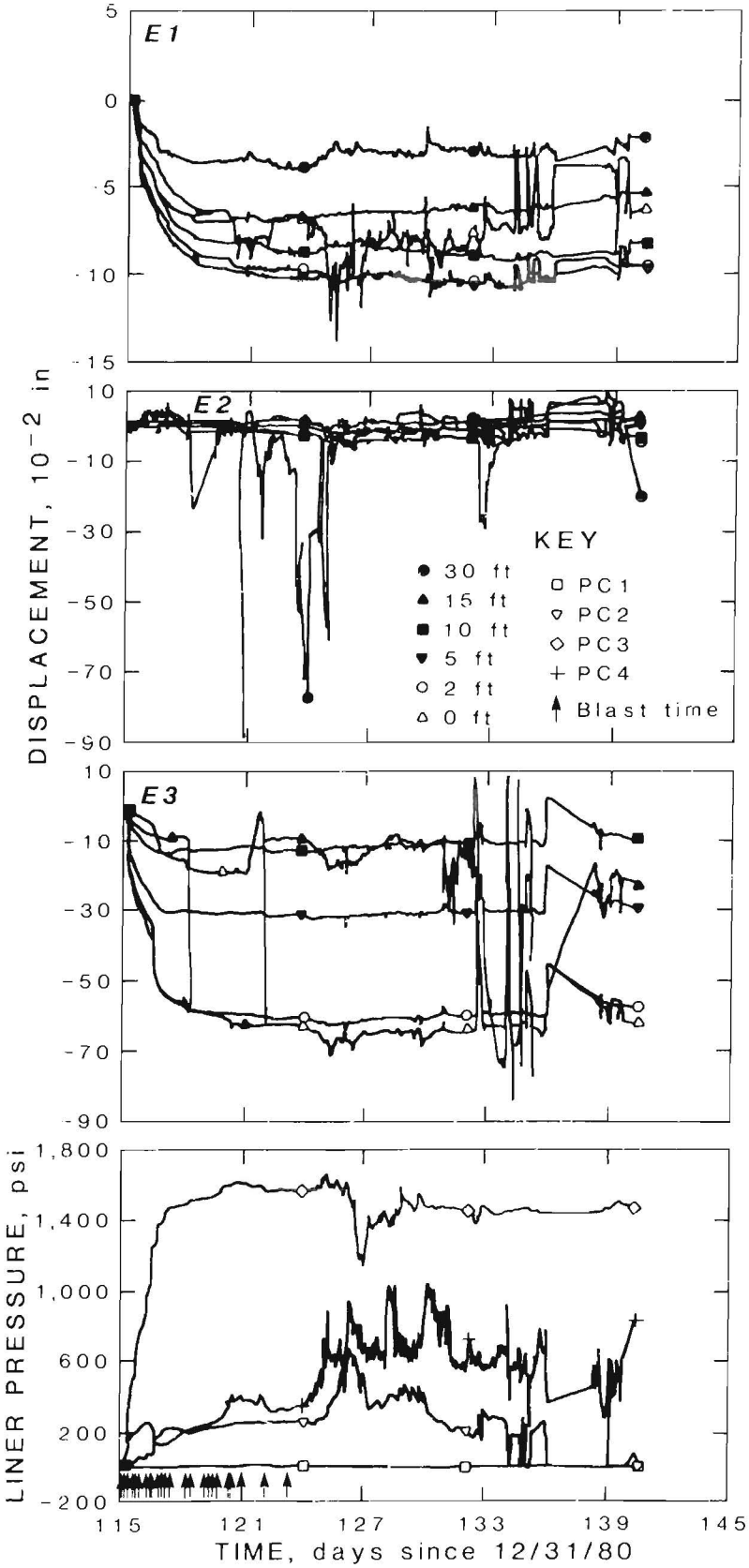

Figure C-3.—2,414-ft depth—30-day displacement and liner stress at each MBPX location *(E-1—E-3)*.

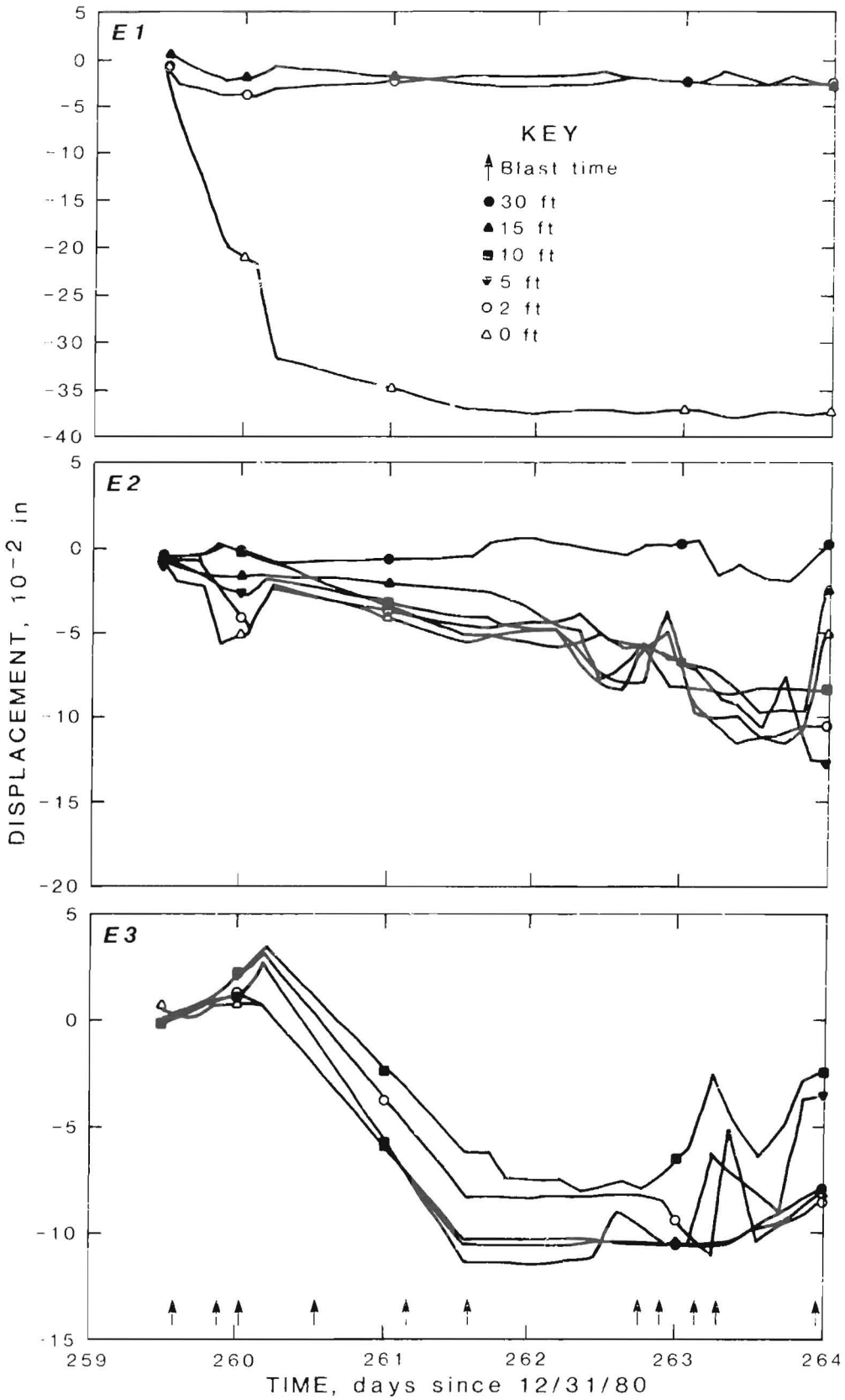

Figure C-4.—4,063-ft depth—5-day displacement at each MPBX location *(E-1—E-3)*.

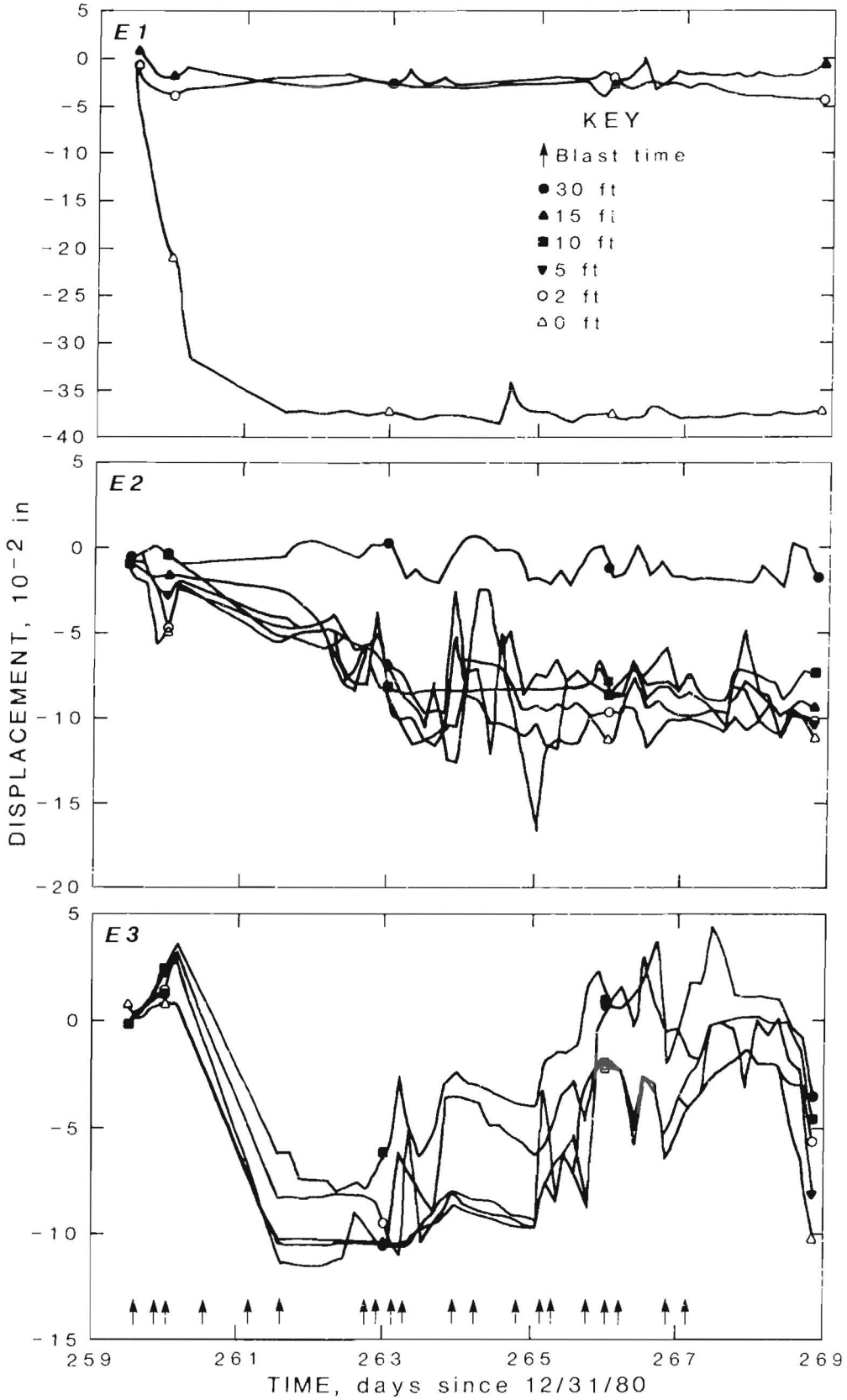

Figure C-5.—4,063-ft depth—10-day displacement at each MPBX location *(E-1—E-3)*.

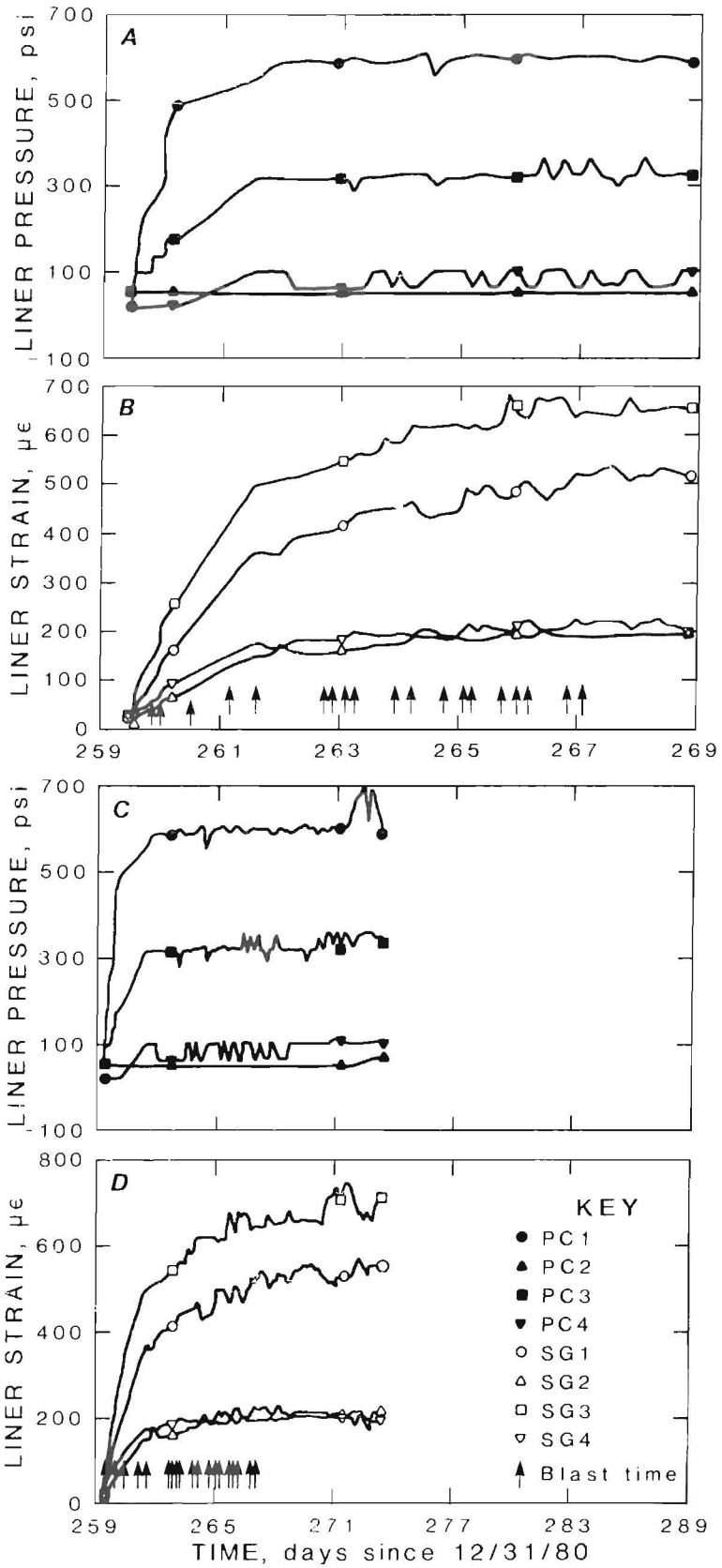

Figure C-6.—4,063-ft depth—10-day liner stress (*A*) and strain (*B*) and 30-day liner stress (*C*) and strain (*D*) at each MPBX location.

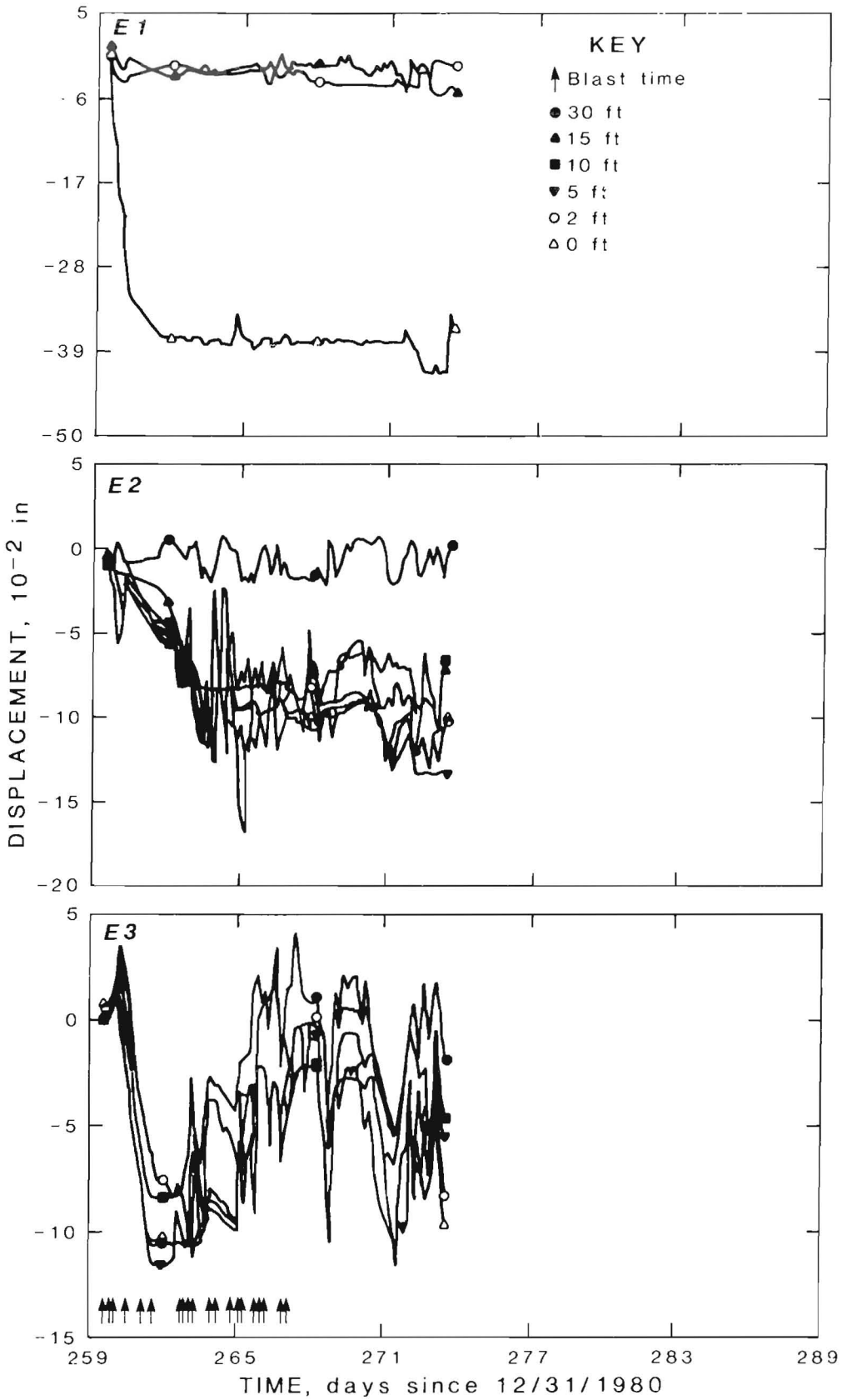

Figure C-7.—4,063-ft depth—30-day displacement at each MPBX location *(E-1—E-3)*.

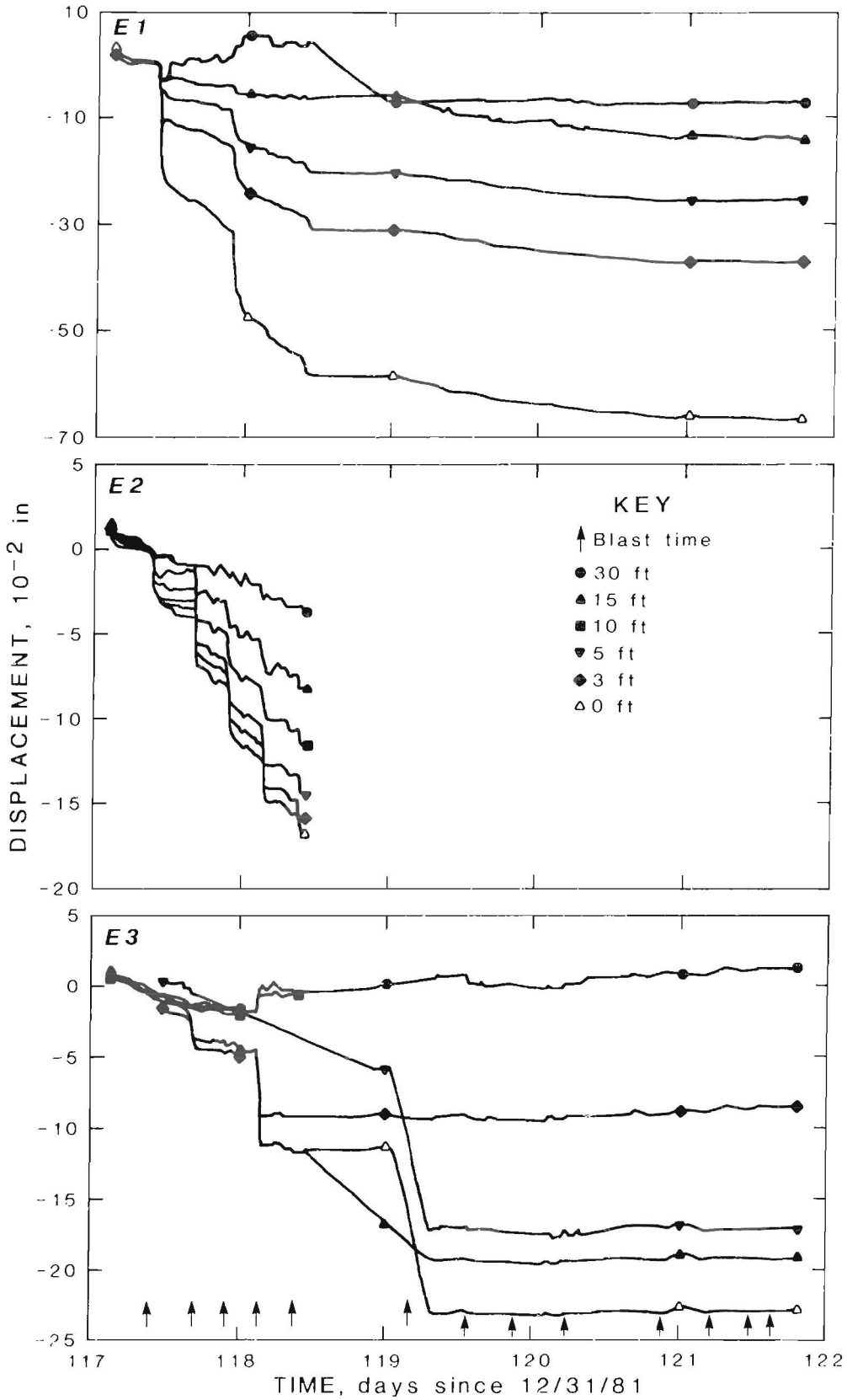

Figure C-8.—5,191-ft depth—5-day displacement at each MPBX location *(E-1—E-3)*.

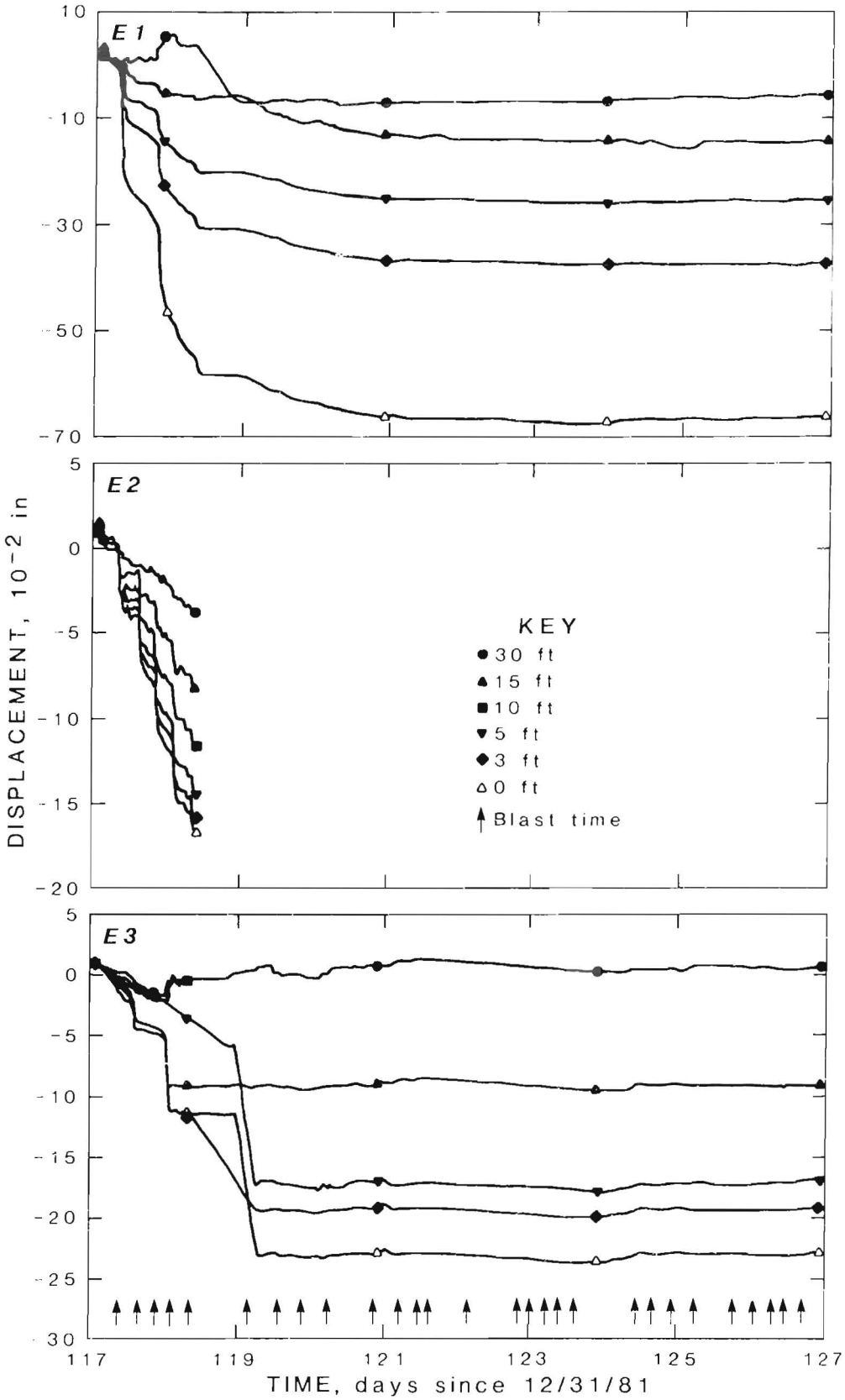

Figure C-9.—5,191-ft depth—10-day displacement at each MPBX location *(E-1—E-3)*.

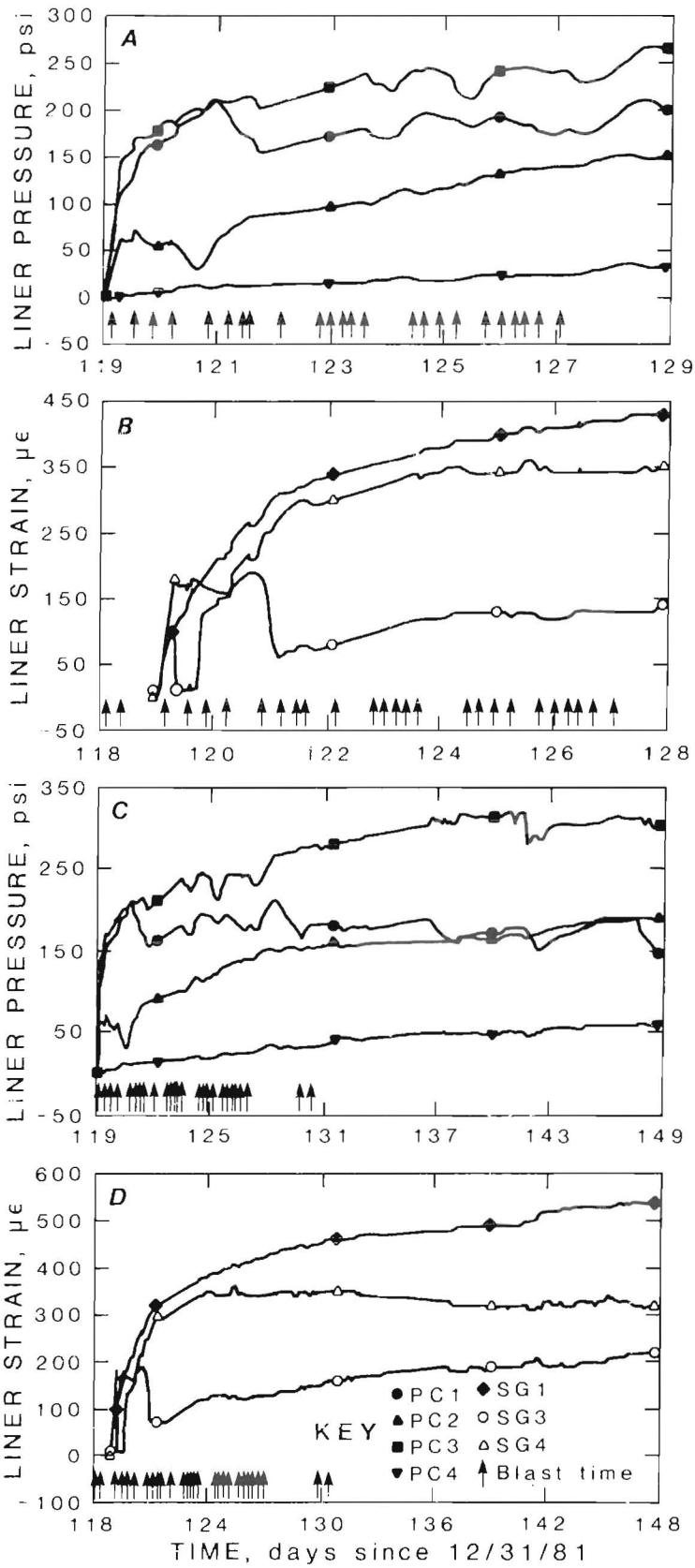

Figure C-10.—5,191-ft depth—10-day liner (*A*) stress and strain (*B*) and 30-day liner stress (*C*) and strain (*D*) at each MPBX location.

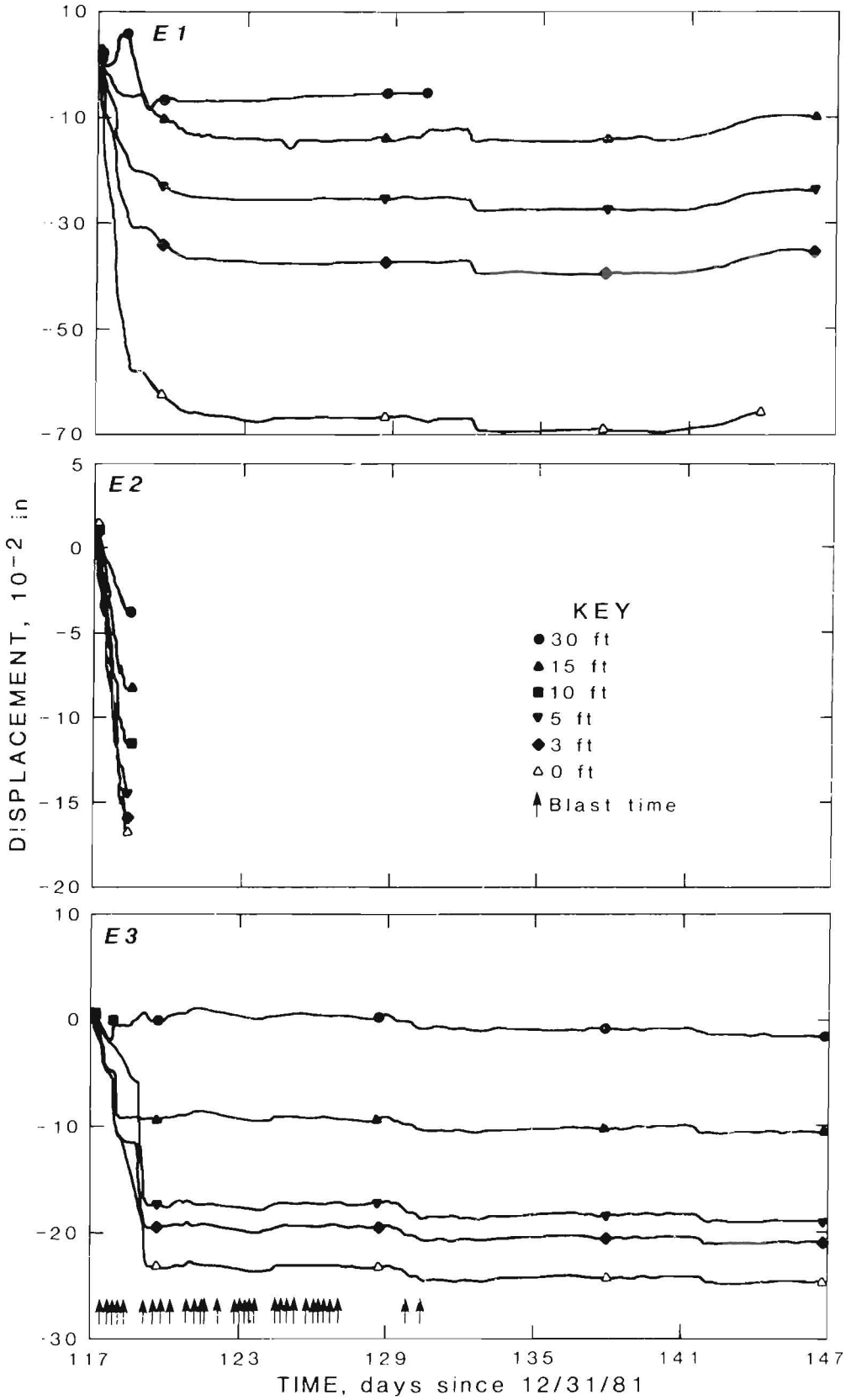

Figure C-11.—5,191-ft depth—30-day displacement at each MPBX location *(E-1—E-3)*.

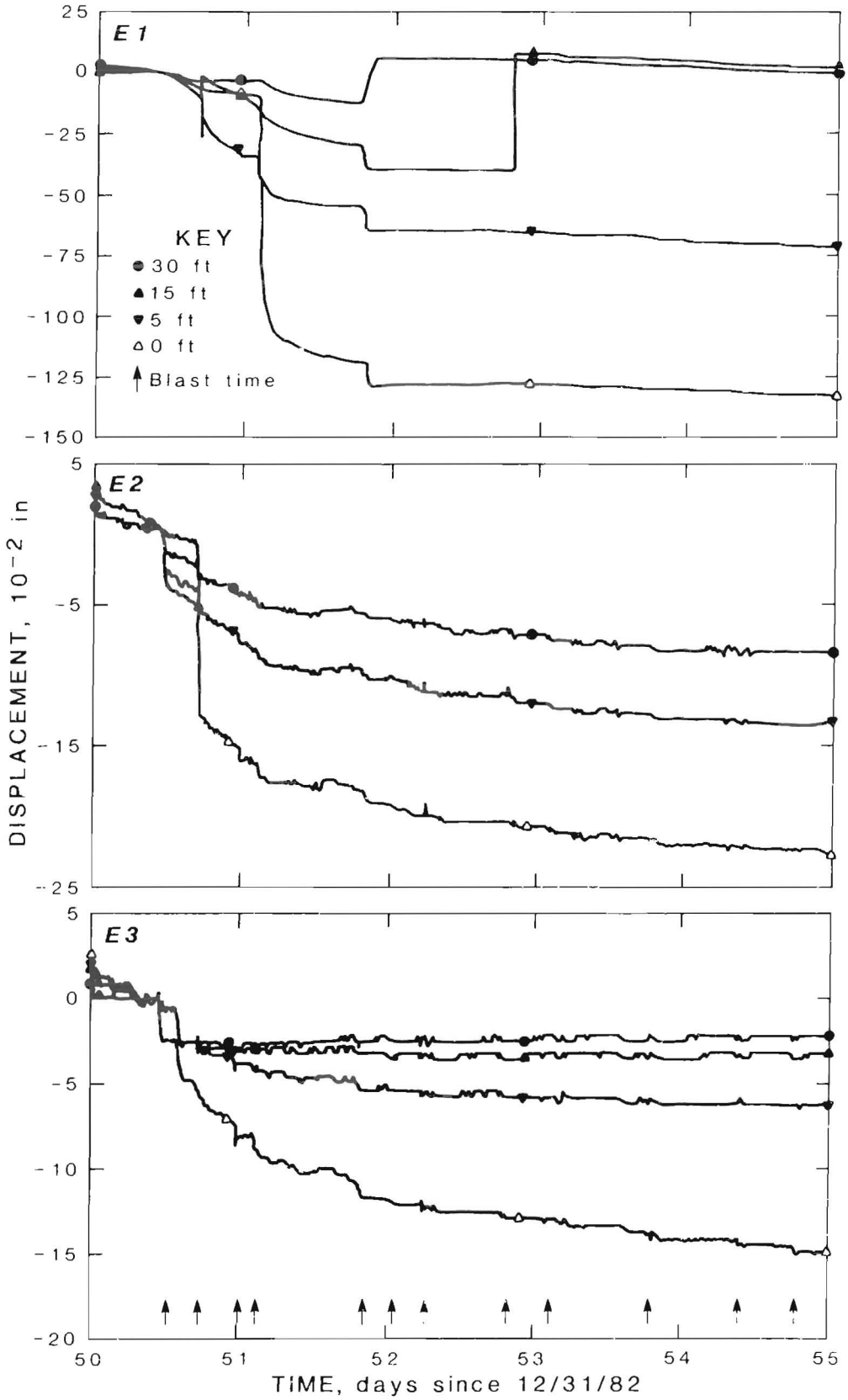

Figure C-12.—5,955-ft depth—5-day displacement at each MPBX location *(E-1—E-3)*.

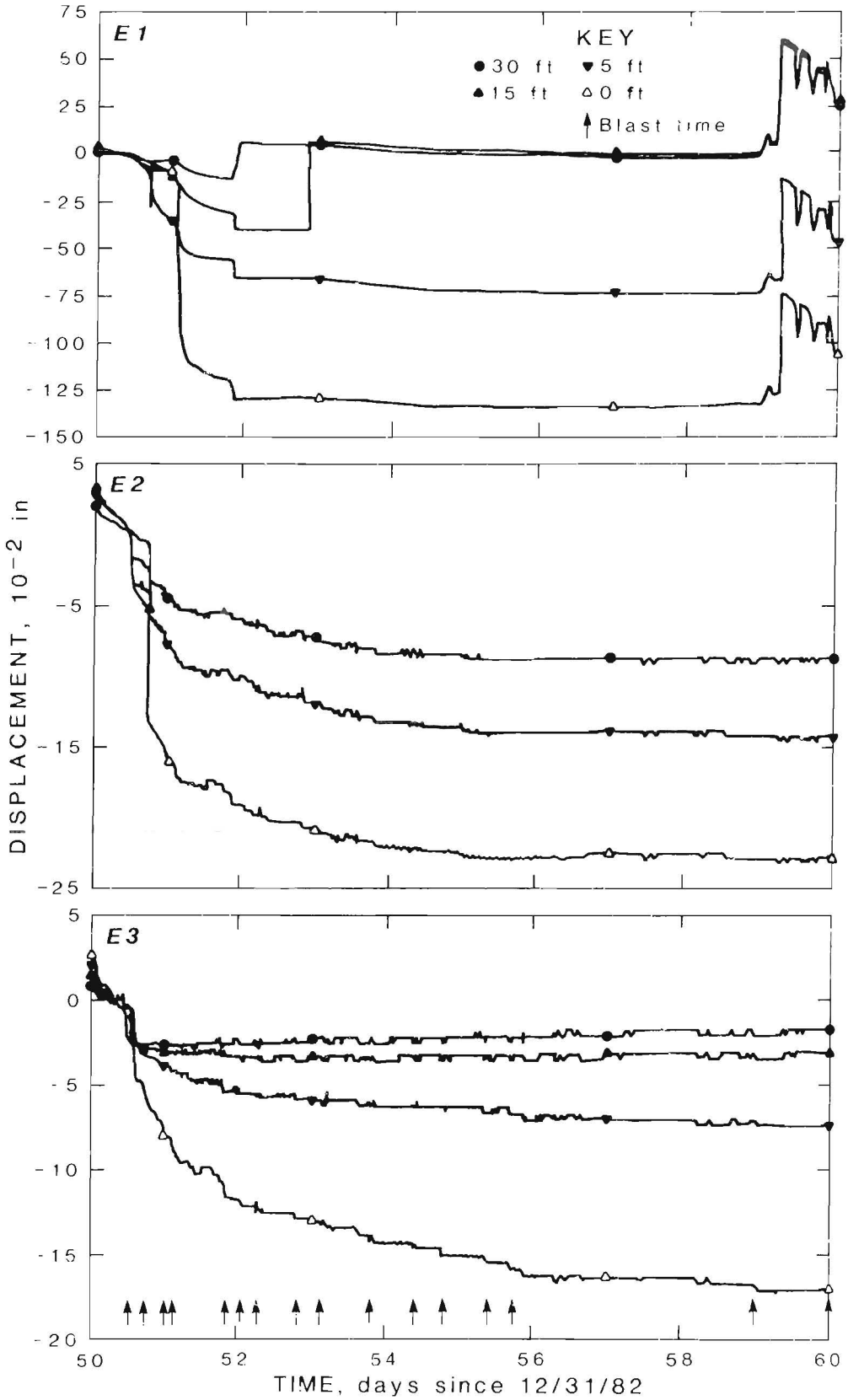

Figure C-13.—5,955-ft depth—10-day displacement at each MPBX location *(E-1—E-3)*.

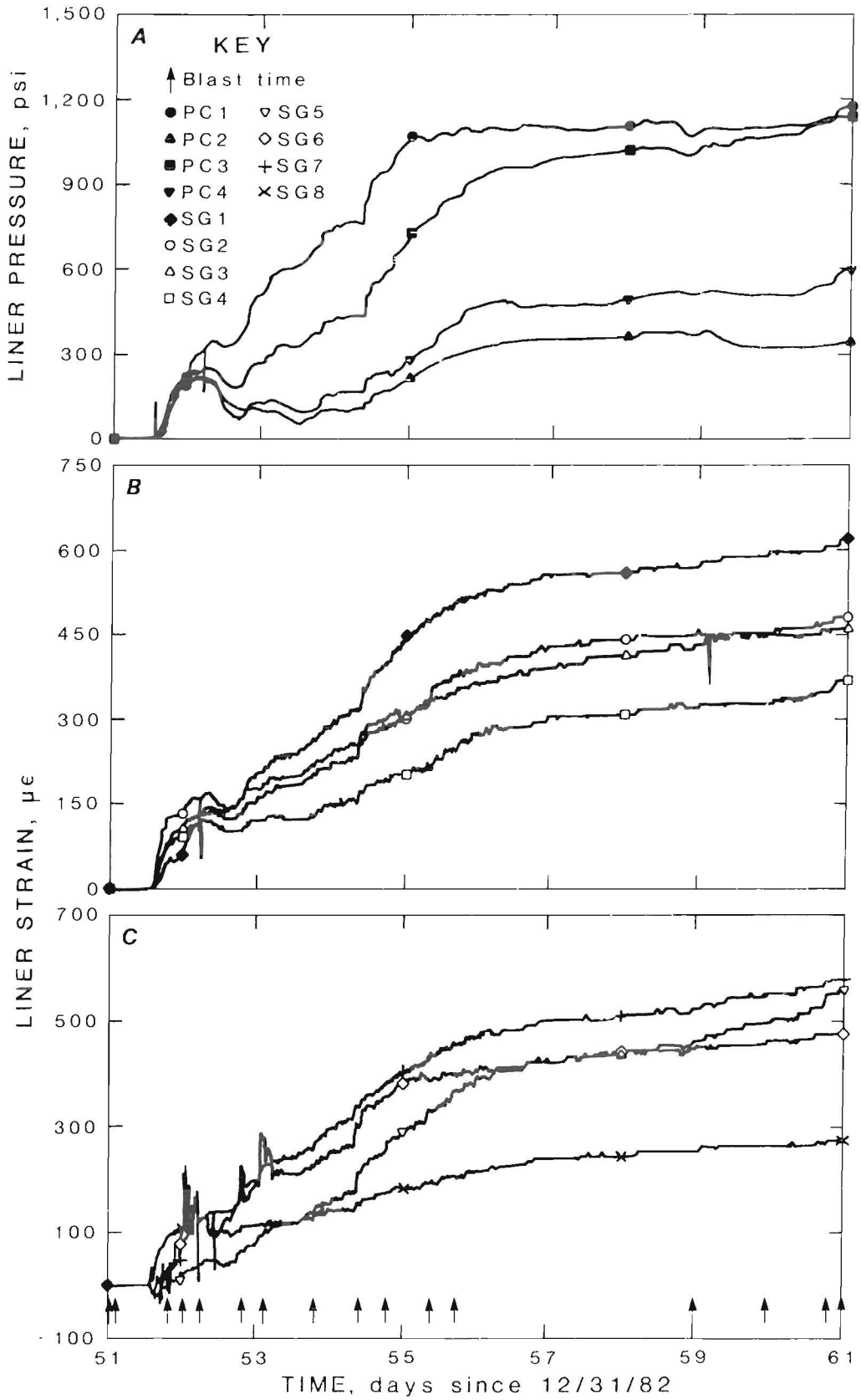

Figure C-14.—5,955-ft depth—10-day liner stress (*A*) and strain (*B-C*) at each MPBX location.

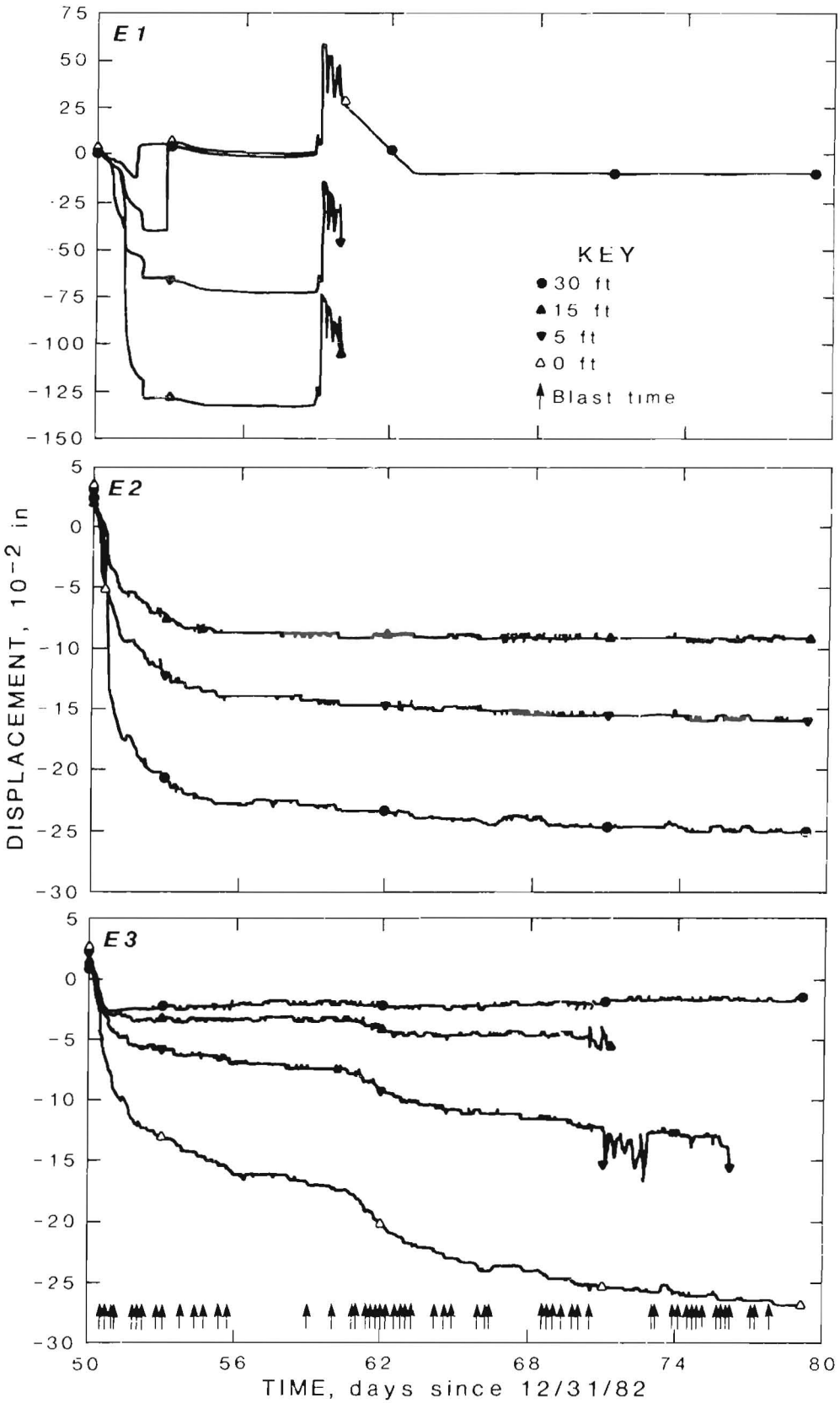

Figure C-15.—5,955-ft depth—30-day displacement at each MPBX location *(E-1—E-3)*.

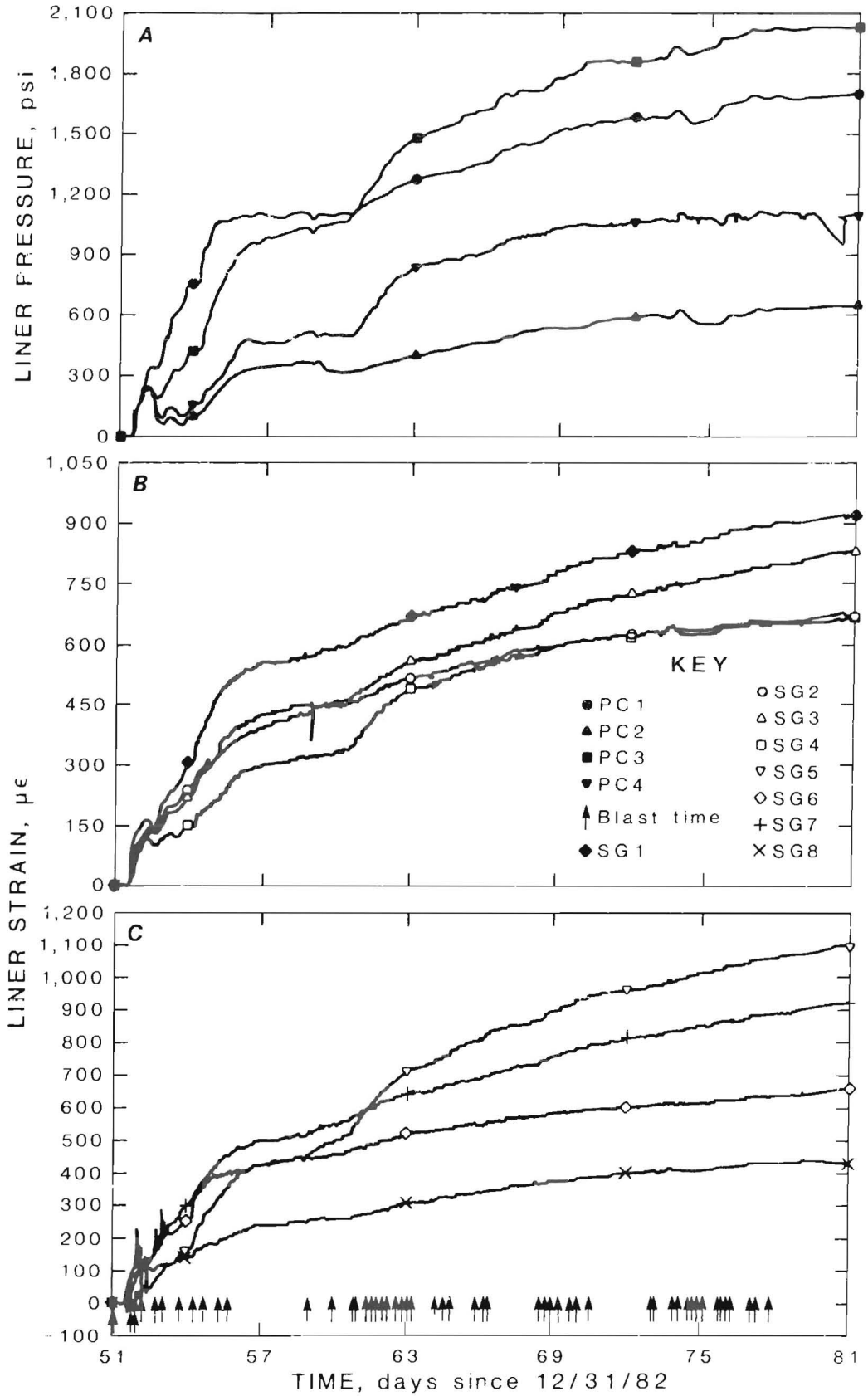

Figure C-16.—5,955-ft depth—30-day liner stress (*A*) and strain (*B-C*) at each MPBX location.

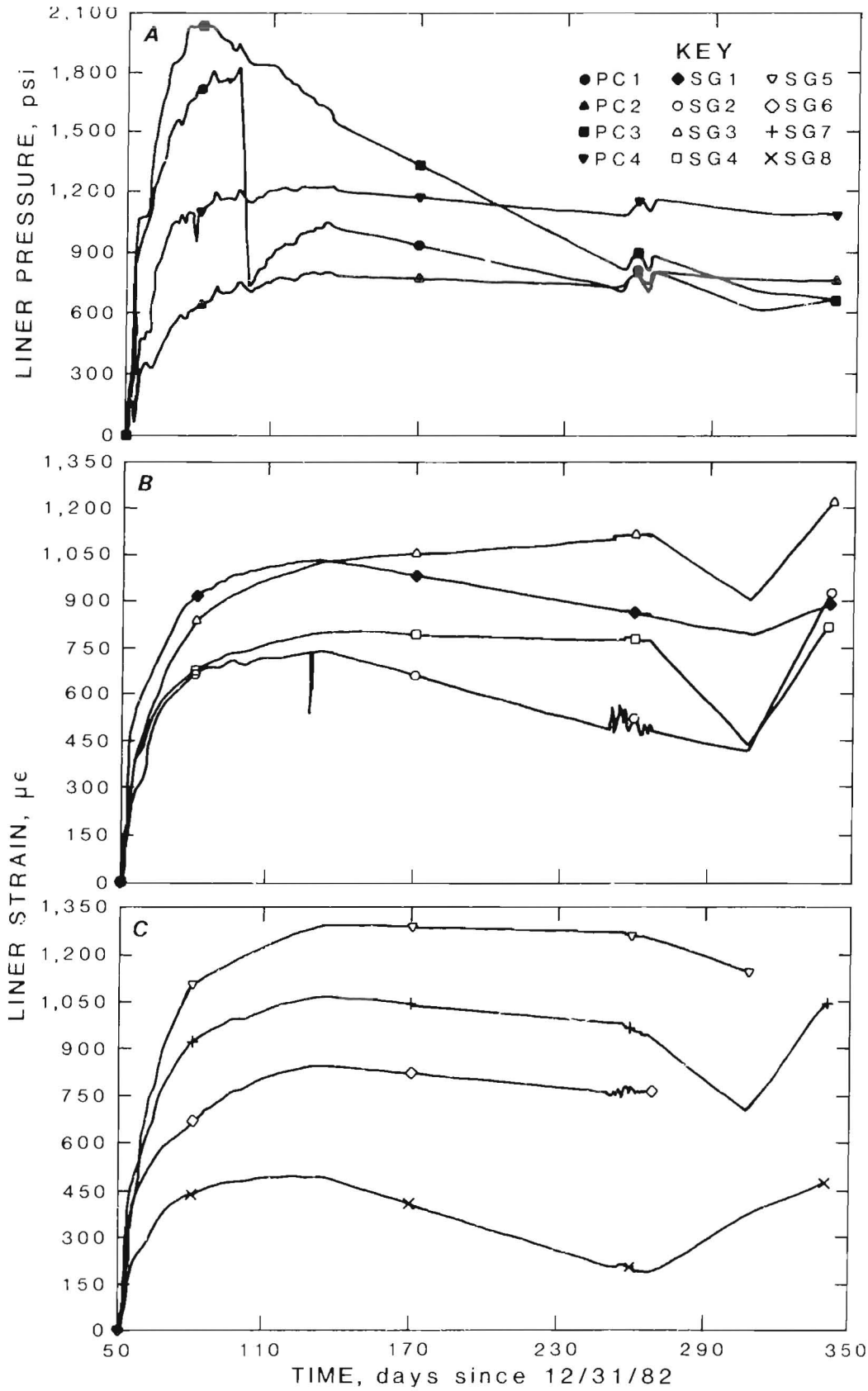

Figure C-17.—5,955-ft depth—300-day liner stress (*A*) and strain (*B-C*) at each MPBX location.

APPENDIX D.–BLAST AND ADVANCE SCHEDULE FOR EACH TEST SITE

TABLE D-1.—Blast and advance schedule for 2,414-ft depth, day 113, 4/23/81

(Install MPBX's and PC's by day 114.6; bottom of shaft at 2,420 ft; elapsed time since 12/31/80)

Blast	Bench	Elapsed time	Shaft bottom, ft	Blast	Bench	Elapsed time	Shaft bottom, ft
1	[1]1	115.22	2,424	13	2	117.55	2,473
2	1	115.29	2,427	14	2	118.28	2,478
3	2	115.50	2,430	15	1	118.52	2,481
4	1	115.67	2,433	16	2	119.20	2,485
5	2	115.83	2,438	17	1	119.40	2,491
6	1	116.03	2,443	18	2	119.60	2,496
7	2	116.33	2,448	19	1	119.85	2,501
8	1	116.54	2,453	20	1	120.40	2,506
9	2	116.65	2,458	21	2	120.50	2,511
10	1	116.95	2,462	22	1	121.00	2,516
11	2	117.12	2,465	23	2	121.20	2,520
12	1	117.30	2,469	24	2	121.30	2,523

[1]North.

TABLE D-2.—Blast and advance schedule for 4,063-ft depth, day 256, 9/10/81

(Install MPBX's and PC's, and SG's by day 225.85; bottom of shaft at 4,067 ft; elapsed time since 12/31/80)

Blast	Bench	Elapsed time	Shaft bottom, ft	Blast	Bench	Elapsed time	Shaft bottom, ft
1	1	259.58	4,072	11	1	263.95	4,119
2	2	259.88	4,077	12	2	264.24	4,124
3	1	260.04	4,081	13	1	264.81	4,128
4	2	260.54	4,086	14	2	265.15	4,133
5	1	261.17	4,091	15	1	265.29	4,138
6	2	261.60	4,095	16	2	265.78	4,143
7	1	262.75	4,100	17	1	266.04	4,147
8	2	262.90	4,105	18	2	266.23	4,152
9	1	263.28	4,114	19	1	266.87	4,155
10	2	263.28	4,119	20	2	267.13	4,162

TABLE D-3.—Blast and advance schedule for 5,191-ft depth, day 116, 4/26/82

(Elapsed time since 12/31/81)

Blast	Bench	Elapsed time	Shaft bottom, ft
INSTALL MPBX'S AT 5,191 ft, DAY 116.90, SHAFT BOTTOM AT 5,200 ft			
1	2	117.40	5,203
2	1	117.69	5,207
3	2	117.91	5,210
4	1	118.13	5,213
5	2	118.38	5,216
INSTALL PC'S AND SG'S AT 5,191 ft; POUR CONCRETE TO 5,193 ft			
6	1	119.17	5,219
7	2	119.56	5,222
8	1	119.88	5,225
9	2	120.23	5,228
POUR CONCRETE TO 5,208 ft			
10	1	120.87	5,232
11	2	121.21	5,235
12	1	121.47	5,239
13	2	121.61	5,242
14	1	122.15	5,245
POUR CONCRETE TO 5,223 ft			
15	2	122.83	5,248
16	1	123.01	5,251
17	2	123.22	5,254
18	1	123.39	5,257
19	2	123.61	5,261

TABLE D-4.—Blast and advance schedule for 5,955-ft depth, day 48, 2/17/83

(Elapsed time since 12/31/82)

Blast	Bench	Elapsed time	Shaft bottom, ft
INSTALL MPBX'S AT 5,955 ft, DAY 49.80, SHAFT BOTTOM AT 5,958 ft			
1	1	48.80	5,958
2	2	50.74	5,965
3	1	51.01	5,970
4	2	51.13	5,975
INSTALL PC'S AND SG'S; POUR CONCRETE TO 5,958 ft			
5	1	51.85	5,980
6	2	52.05	5,983
7	1	52.27	5,985
8	2	52.83	5,987
9	1	53.12	5,991
9a	[1]6000	53.80	NAp
9b	[1]6000	54.40	NAp
10	2	54.78	5,994
10a	[1]6000	55.40	NAp
POUR 88 yd^3 CONCRETE TO 5,973 ft			
11	[1]6000	55.74	NAp
11a	[1]6000	NAp	NAp

NAp Not applicable.

[1]Station.

◦ U.S. GOVERNMENT PRINTING OFFICE. 611-012/00,052

INT.-BU.OF MINES,PGH.,PA. 28877